Measuring cycling kinematics using a low-cost, flashing LED, multi-camera approach

by

Matthew Gilbertson

SUBMITTED TO THE DEPARTMENT OF MECHANICAL ENGINEERING IN PARTIAL FULFILLMENT OF THE REQUIREMENTS FOR THE DEGREE OF BACHELOR OF SCIENCE IN MECHANICAL ENGINEERING
AT THE
MASSACHUSETTS INSTITUTE OF TECHNOLOGY
JUNE 2008

Signature of Author:_____
Department of Mechanical Engineering
May 12, 2008

Certified by:_____
David J Willis
Research Scientist, MIT Dept of Aeronautics and Astronautics
Thesis Supervisor

Accepted by:_____
John H. Lienhard V
Professor of Mechanical Engineering
Chairman, Undergraduate Thesis Committee

Measuring cycling kinematics using a low-cost, flashing LED, multi-camera approach

by

Matthew Gilbertson

Submitted to the Department of Mechanical Engineering on May 12, 2008 in partial fulfillment of the requirements for the Degree of Bachelor of Science in Mechanical Engineering

ABSTRACT

In this thesis a low cost motion capture approach is presented and applied to measure cyclists' kinematics. The motion capture system consists of low cost hardware and custom developed software. Based on still-frame, off-the-shelf digital cameras, the method represents a solution which is accessible to the average athlete. With the exception of off-the-shelf digital cameras the total cost of the hardware is less than $100.

The motion capture system is applied to study cyclist kinematics for three different types of bicycles: road bikes, triathlon bikes, and mountain bikes. Coupled with power output measurement and wind tunnel drag measurements, the investigation of several different standard cycling positions is performed. The results indicate a significant component of out-of-plane joint motions, especially in the knee, with an average knee excursion between 0.15" and 0.21". The system was also used to measure cycling cadence, with a range between 1.06Hz and 1.63Hz. Joint angle analysis suggested a positive correlation between ankle angle range and power output. Further in-depth analyses of these data or similar data collected using these motion capture approaches may give deeper insight into which motions correlate with higher power outputs. Wind tunnel and power data were used to calculate position transition velocities for different exertion levels and hill angles. This low-cost system was demonstrated to be a useful and effective tool for measuring and analyzing cycling kinematics.

Thesis Supervisor: David J Willis
Title: Research Scientist, MIT Department of Aeronautics and Astronautics

Table of Contents

Acknowledgements

I would like to thank David Willis and Eric Gilbertson for their endless help in this entire experiment. I would also like to thank Zach LaBry for his help in operating the Wright Brothers Wind Tunnel and in facilitating the borrowing of equipment. I would like to also thank Jim Bales from the Edgerton Strobe Lab for suggesting the LED-based idea. Finally, I would like to thank all of the participants in this study for their help and cooperation.

Preface

This work was performed under MIT COUHES (Committee On the Use of Humans as Experimental Subjects), Protocol # 0803002675. Three experimenters helped in the gathering of data: Matthew Gilbertson, Eric Gilbertson, and David Willis. Each member of the experimental data collection team had taken the MIT online human subjects training class and received COUHES approval. This work was partially funded by the MIT UROP office.

Chapter 1: Introduction

The human body is capable of finely controlled skeletal motions making the practice of sports a physical challenge at all levels of competition. These changes in shape are governed by the complex interactions of the musculoskeletal system. Three-dimensional reconstruction of human body kinematics can provide information about variability in task performance and insights for objective driven modifications (some examples include kinematics analysis for bicycle fit, modification of the golf-swing mechanics for better performance and baseball-pitcher motion analysis).

Human motion tracking is currently reserved for high performance athletes as well as gaming and animation applications due to the significant cost of motion capture/tracking systems and the need for specialized analysis tools. Many motion capture systems require the use of high frame rate digital cameras (200fps or more eg: Vicon Motion Capture Systems [1]), full body suits with six-degree of freedom accelerometers [2], or a complex system of infrared light emitting diodes and sensors (the Retul System [3], discussed more in Section 1.1.1). This thesis explores a low-cost alternative for motion capture which uses flashing LED's and still frame cameras to record the data and a series of simple, custom developed Matlab codes to process and analyze the data.

Cycling is a well controlled, yet sufficiently complex test case for motion capture and kinematics analysis. On a stationary bicycle or trainer, the cyclist's motions are constrained and the periodic data is easy to collect. Furthermore, the kinematics of cycling can be simplified to the periodic relative motion of a series of bars and linkages. In addition to being a challenging test case in the laboratory environment, cycling has received significant interest from both amateur and professional athletes. Compelled by this interest in cycling, a significant amount of research has been conducted to find optimal cycling positions [4]. In this work we present an approach which examines the recommended cycling positions, while measuring kinematics, power output and drag. Furthermore, the motion capture system which is presented is a low-cost system that uses off-the-shelf digital cameras and simple circuitry to flash Light Emitting Diodes (LEDs) at high frequency.

1.1: Background

Measuring body dynamics using motion capture systems involves capturing joint motions from more than one viewpoint and reconstructing the three-dimensional motion based on stereographic principles. Image capture systems can take many forms, from active (Retül) to passive markers (Vicon), from high frequency strobes (the MIT Edgerton Center) to high frame rate motion cameras.

1.1.1 Motion Capture Approaches

Several systems exist to measure body kinematics while cycling. The most similar approach to the method we propose is the commercially-available Retül System [3] which is an active-marker motion capture system. The Retül system uses a series of eight infrared LEDs that flash at 476Hz. These high frequency infrared flashes are detected by two infrared sensors placed several feet away from the subject. The system computes the locations of the joint markers and the resulting motions and bike-fit must be interpreted by a trained bike fitter. The approximate cost of the complete system is $10,000 [5].

High speed photography can also be used to analyze cycling kinematics [1]. High speed digital cameras simplify the process used for calculating 3D positions and are capable of capturing images at high rates (approximately 10Hz-10,000Hz); however, these systems are expensive and typically have lower resolution than average amateur digital cameras when motion capture occurs at high frame rates. Furthermore, to capture motion accurately, the digital moving picture cameras used in the three-dimensional coordinate reconstruction must have synchronized shutters. This shutter synchronization requirement is difficult to satisfy using most off the shelf digital camcorders, resulting in increased system cost.

Another system that can be used to measure cycling kinematics is based upon the strobe light concept. Bright pulses of light are flashed at high frequencies on cyclist and images recorded. A similar system has been used in the MIT Edgerton Strobe lab to capture sports images such as golf swings and football kicks.

These first two approaches are expensive and typically are reserved for professional athletes. In this thesis a low-cost alternative that can be built for less than $100 is presented. The system consists of digital still-frame cameras and a flashing LED circuit which is described in detail in Section 2.5. In the proposed motion capture system, high frequency LED flashes are recorded on the digital image sensor as discrete dashes of light on the photograph. By attaching the LEDs to the cyclist's joints, a time dependent streak is generated in the image representing the motion of the joint/LED (illustrated in Figure 1). Simple custom software is used to track the LED flashes in the photograph. These two-dimensional recorded image-coordinates are subsequently transformed to three dimensional locations using stereo-imaging approaches in order to quantify the actual motion of each LED.

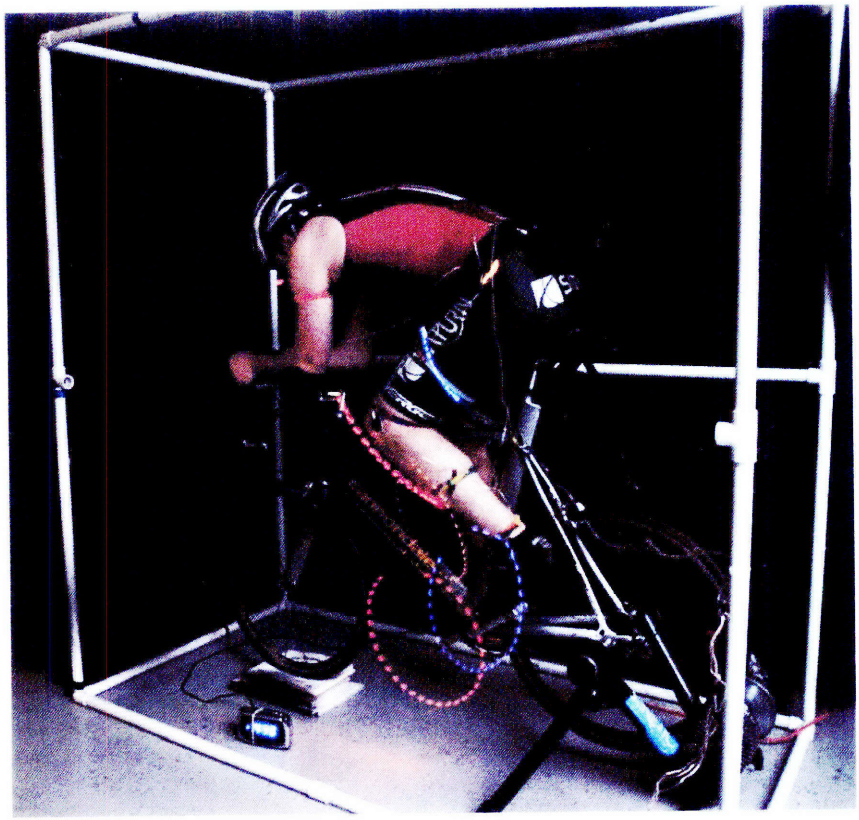

Figure 1: An illustration of the flashing LED circuit attached to a cyclist's leg. Notice in this photograph that the LED traces provide an accurate, time history of the location of the leg joints. In the actual experiment, the light in the room is reduced in order to record the LED traces without significant image clutter.

Note: the photograph in Figure 1 and the rest of the photographs in this thesis show models used to demonstrate the experiment. Due to privacy and confidentiality, none of the photographs represent actual data taken during this experiment.

1.2 Analysis of Different Cycling Positions

The proposed motion capture approach is applied to the analysis of cyclist kinematics. In this experiment we demonstrate that this system works in each of the standard positions a cyclist assumes. In addition, we use the system to demonstrate the benefits of acquiring time-dependent cycling kinematics data.

1.2.1 Previous work:

This thesis focuses on the motions of four joints and their associated joint angles: the ankle, hip, knee, and shoulder (see Figure 2). As the cyclist pedals, the torso moves very little, while the thigh executes a sweeping arc due to the constraints imposed by the hip joint and bicycle seat, creating a time varying hip angle (HA). The knee angle (KA) and ankle angle (AA) also vary in a manner similar to a five bar-linkage system with the foot constrained to the pedal-crank system. This makes the HA, KA, and AA the primary parameters affected by bike shape and body position.

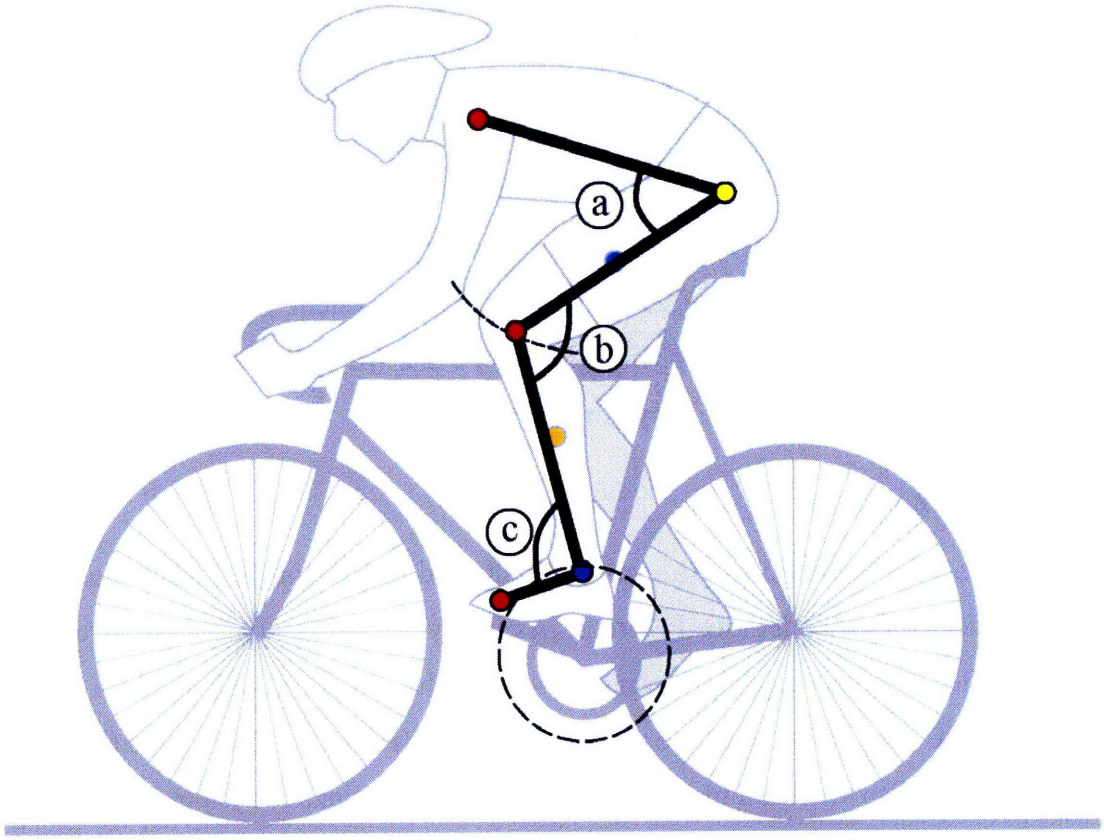

Figure 2: The joint angles measured in this experiment. (a) is the hip angle, (b) is the knee angle (c) is the ankle angle. These angles are all measured with respect to the known positions of the joint LED markers.

Several researchers have performed work related to the kinematics of bicycling. Heil [6] studied the relationship between biological factors, namely, the heart rate and respiratory rate for different bicycle geometries and cycling kinematics. Heil approximates the seat tube, crank, foot, tibia, and femur as a closed five-bar linkage. Using pure geometry considerations, he approximates the kinematics of the leg. This assumes that the leg motions are constrained to a 2-dimensional plane and that the hip is a stationary joint. The proposed system captures cycling kinematics more accurately and fully by recording the time-history of the joint motions, out-of-plane cycling motions and small changes in the hip and shoulder position. By recording the time-varying motion of the joints, the actual time varying angles are determined, reducing the uncertainty introduced by static angle measurements and simplified two-dimensional bar-linkage approximations.

Chapter 2: Motion Capture Hardware

The hardware used to capture images in this experiment consists of six primary systems:

1. Circuitry: The LED Circuit, the LED Flashing Circuit, and the Switching Circuit.
2. Three standard digital cameras: A Canon Digital Rebel D300 SLR, an Olympus Camedia D580, and an Olympus Stylus 770SW.
3. Two custom shutter release mechanisms that enabled a single experimenter to capture simultaneous photographs from well separated cameras.
4. A *Kinetic* fluid cycle trainer.
5. A PowerTap [7] wheel that measured power output and speed.
6. A calibration frame and associated circuitry.

Each of these systems and its associated subsystems are described in the sections that follow.

2.1 Circuitry

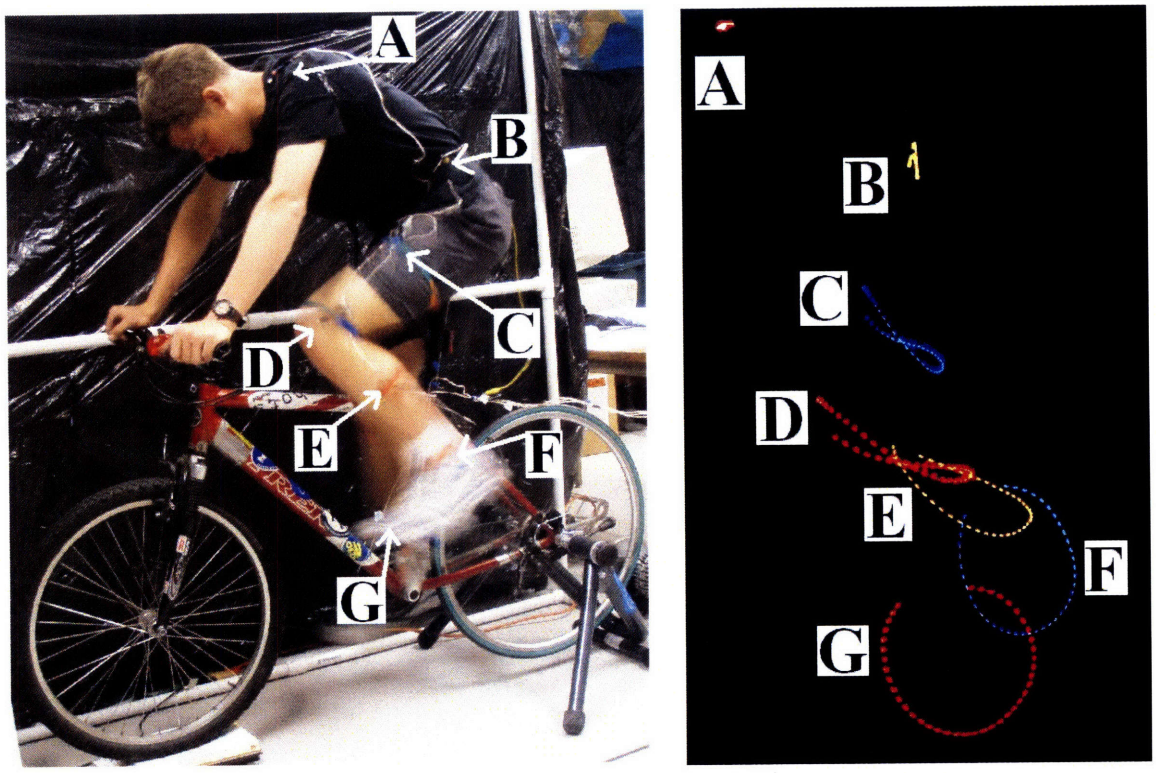

Figure 3: A cyclist shown with LED Circuit attached (left). Discrete LED Flashes produced by LED Flashing circuit (right) with room lights off.

2.2 Overall circuit operation

The circuitry which produces controlled flashing LED time traces on the exposed photograph consists of three circuits: a multi-colored LED circuit that is attached to the cyclist's leg (the LED Circuit), a circuit that is used to generate a series of equal duration, high frequency signals which generate the LED flashes (the Flashing Circuit) and a series of switching circuits that are used to turn the flashing LED circuit on and off (the Switching Circuit). In this experiment the two switches S1 and S2 are mounted to down tube and seat post of the bike, respectively (see Figure 9). The combination of switch S1 to turn on the LEDs and switch S2 to turn off the LEDs enables the LEDs to flash in a controlled manner for a nearly complete cycle. A circuit diagram is shown in Figure 4. A photograph of the overall circuit is shown in Figure 5.

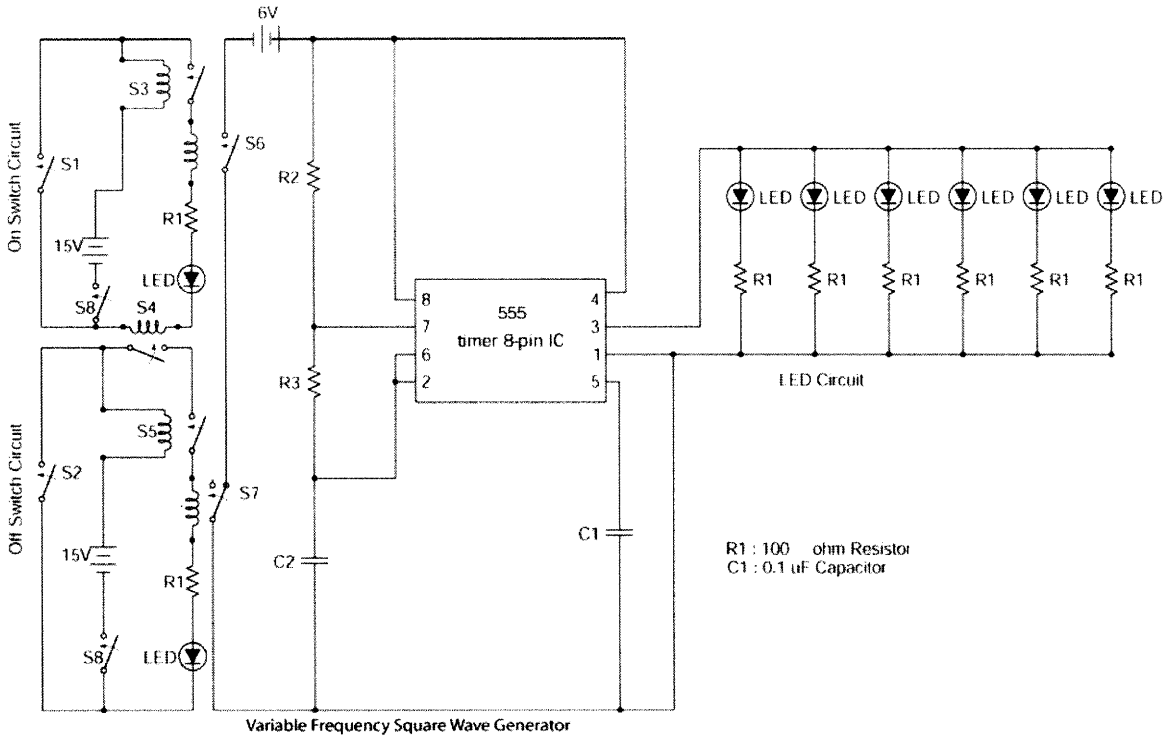

Figure 4: Circuit diagram showing the switching circuit (left), the flashing circuit (center) , and LED circuit (right)

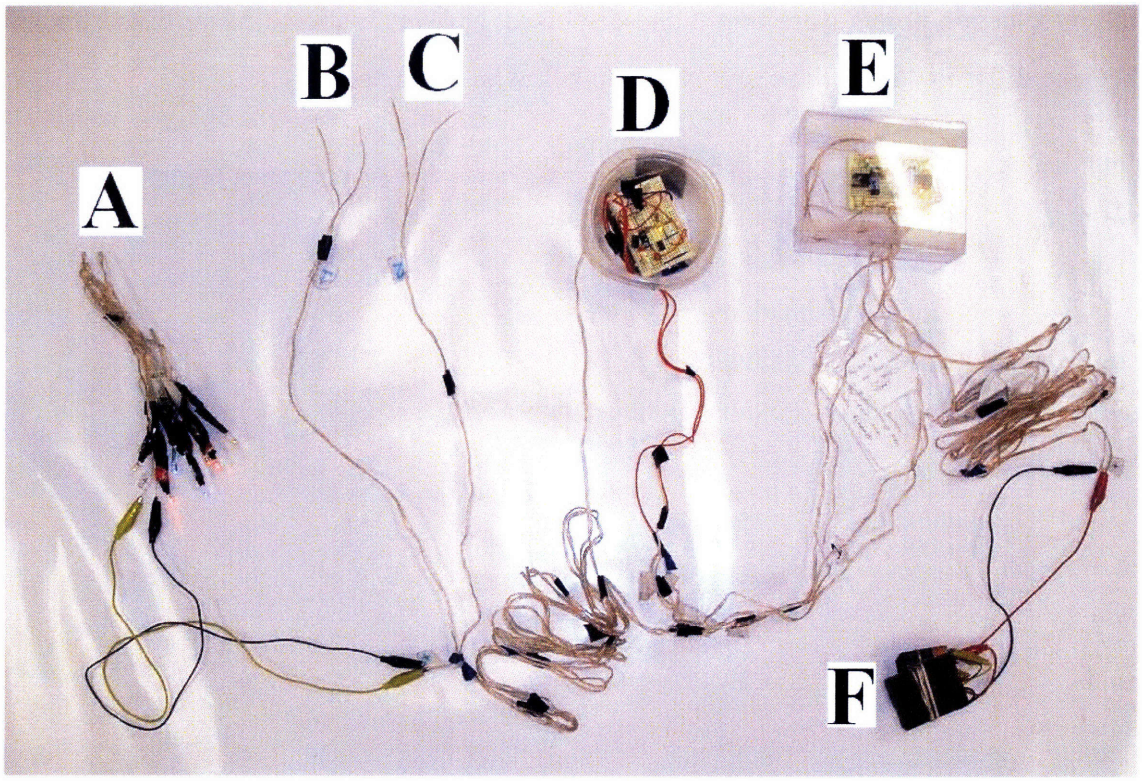

Figure 5: The overall circuit, showing (A) the LED Circuit, (B) Switch 1, (C) Switch 2, (D) the Flashing Circuit, (E) the Switching Circuit, and (F) the 15V battery pack used to arm/disarm the circuit

2.3 The LED Circuit

The LED circuit comprises the active markers in the motion capture system. To be an effective marker system, the individual LED flashes must be bright enough to be captured by the cameras in a darkened room. In addition, the circuit has to be easily attached to and detached from the subject's leg. The system was developed through the iterations described below.

Iteration 1: Using Optical Lines to Connect LEDs

In early tests, the paths of two series of recorded LED flashes often overlapped and the two overlapping streaks became indistinguishable. An optical element that connected the LEDs was devised. A transparent, flexible drinking straw was used to connect two similar-colored LEDs. The inside of the straw was abraded to introduce scratches to disperse the light along the length of the straw. This system effectively eliminated the problems caused by overlapping traces; however, when multiple lines of light overlapped,

the intersection points were bright and dispersed, and automatic software based tracking became difficult. A sample result is shown below in Figure 6.

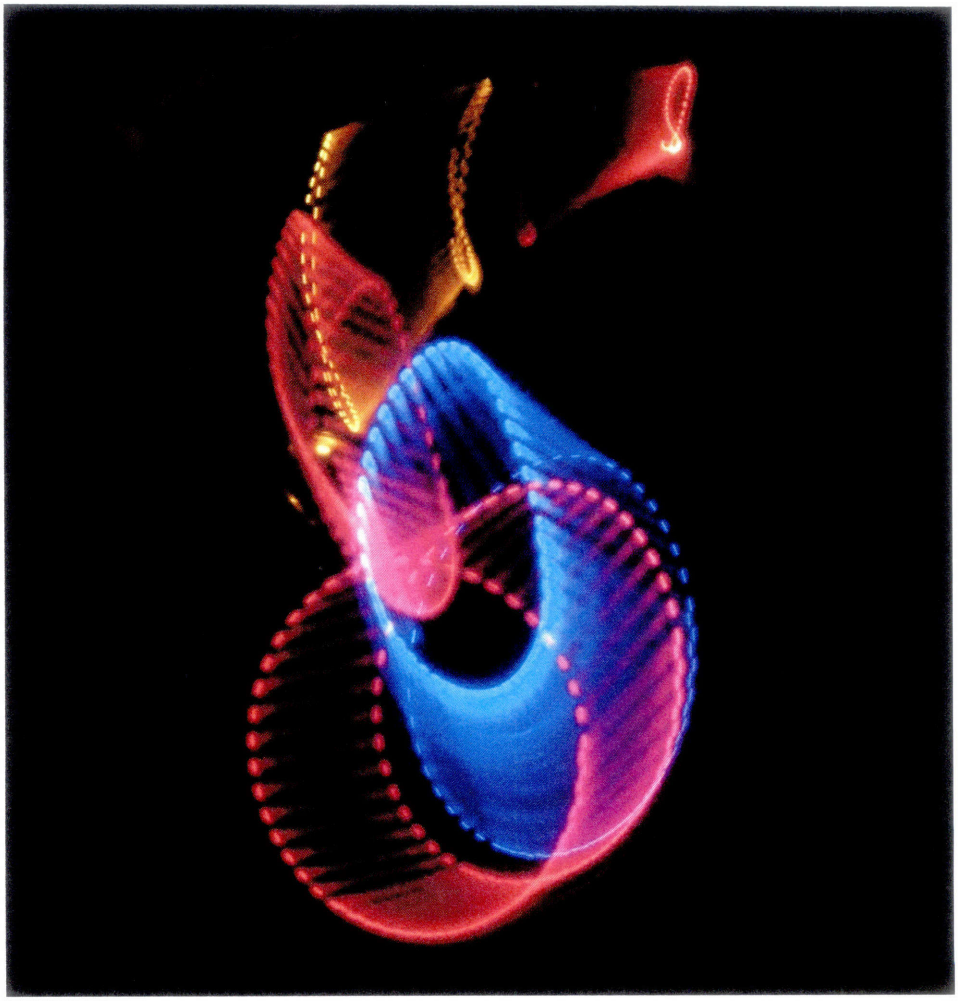

Figure 6: First iteration of the LED Circuit, with the LEDs connected by transparent straws to disperse the light down a line. Note the excessive blurring that occurs when two streaks overlap.

Iteration 2: A bare, seven LED circuit

Due to the challenges introduced in the automatic tracking, the straws were removed from the system, and the total number of LEDs was reduced to seven (toe, ankle, calf, knee, thigh, hip, shoulder). Three colors of LEDs were used: red, blue, and yellow. Six of the LEDs were soldered in parallel and placed equidistantly on a 3 ft long wire (see Figure 7 below). A seventh LED was connected in parallel and led to the shoulder. Appropriate resistance was added in series to ensure all seven LEDs had similar brightness. Each LED / resistor combination was fitted with a small plug, which allowed

the LEDs to be easily connected and disconnected from the circuit. The LED system was wired to the Flashing Circuit (see Section 2.5) with a 6V input voltage. The LED system was attached to the subject's legs using Velcro so that each LED pointed outwards, towards the cameras. Some LEDs were taped down to reduce movement.

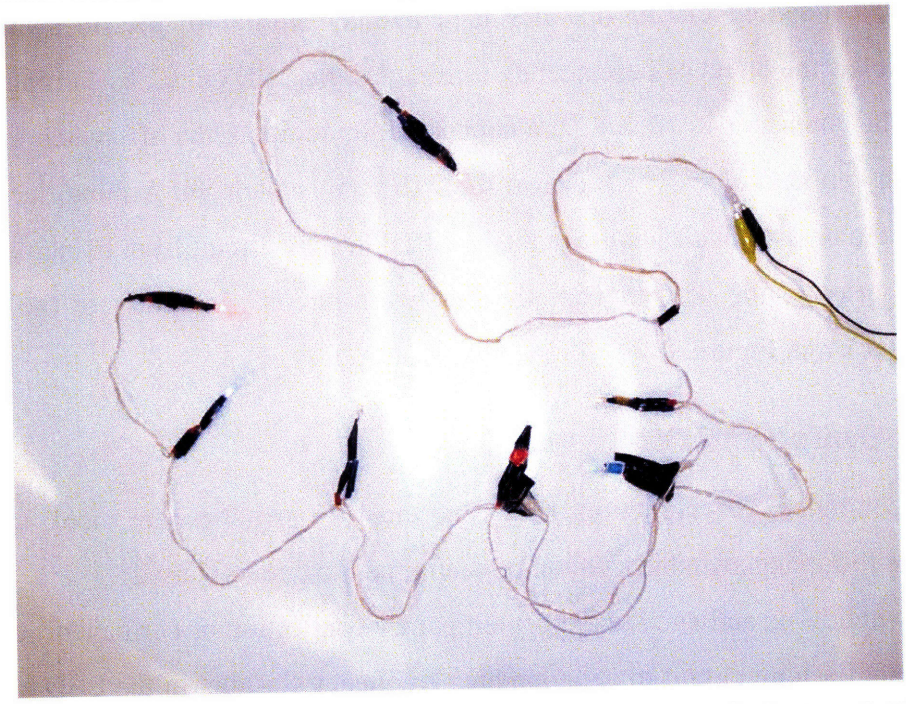

Figure 7: The LED circuit. The top LED is attached to the shoulder and the bottom six LEDs, with alternating colors, are attached to the leg.

2.4 The Switching Circuit

The flashing LED circuit was controlled by a switching circuit to capture a nearly complete, single pedal stroke during the period when the shutter was open. Initial manual on/off switching circuits were found to be unreliable and inconsistent, often producing LED light trails much less than or much more than a single pedal stroke. A switching circuit was developed in order to control the activation and deactivation of the LED flashing circuit.

2.4.1 On-Switch Circuit Description

The on-switch circuit is designed to activate the LED flashing circuit via Switch S6, when the contacts of switch S1 make a connection. When switch S1 is activated, the relay-switch S3 is also turned on activating the relay switch S6 which turns on the LED flashing circuit. Due to the activation of the relay switch S3, subsequent closing and

opening of switch S1 will not affect the state of switch S6. The on-switch, once activated, turns on switch S6 permanently until the circuit arming switch, S8, is deactivated.

2.4.2 Off-Switch Circuit Description

The off-switch circuit operates in a manner similar to the on switch circuit; however, it has the effect of permanently turning off the LED circuit by turning switch S7 off when the contacts of switch S2 are connected. In addition, the off-switch circuit must be armed by an active on-switch circuit through relay switch S4. Arming the off-switch circuit via the on-switch circuit prevents the LED flashing circuit from being permanently turned-off prior to the activation of the on-switch circuit. A picture of the Switching Circuit is shown in Figure 8.

2.4.3 On-Switch and Off-Switch Operation

The combined permanent-on and permanent-off-switches are used together to achieve the following switching sequence each time the circuit is used:

1. Switch S1 is activated (can be a temporary connection or permanent) causing the LED flashing circuit to generate high frequency flashing in the LED circuit. Any prior activation of switch S2 has no effect on this initial activation.
2. Switch S2 is activated (temporarily or permanently) causing the LED flashing circuit to turn off permanently. Subsequent activation of switch S1 or switch S2 has no effect.
3. Switch S8 is used to reset the permanent-on and permanent-off-switches to their original state.

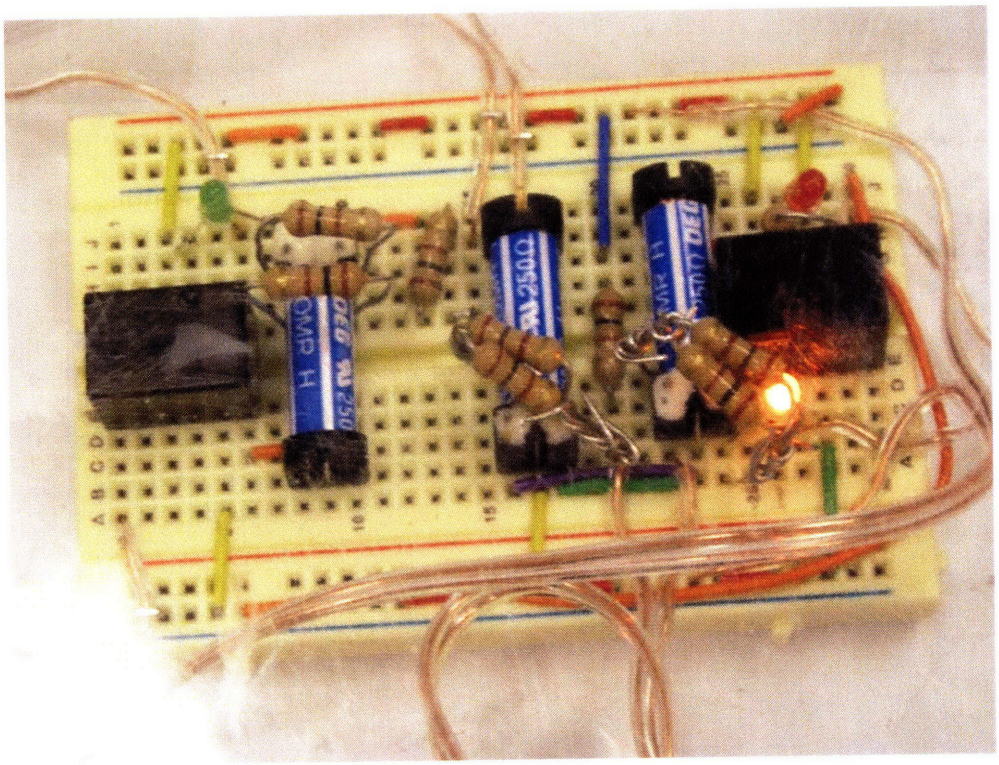

Figure 8: The switching circuit

2.4.4 Switching circuit installation

In order to turn the LED system on for the desired interval of less than one pedal stroke, the switching circuit is installed on the seat tube and the down tube of the bike's frame, shown in Figure 9. S1, which consists of two copper wires, bare on the ends, is attached to the down tube of the bike so that the bike's left crankarm contacts the two bare ends while the cyclist is pedaling. S2 is attached in a similar manner to the bike's seat tube. A small piece of Aluminum foil is then attached to the left crankarm to enhance its electrical conductivity. Thus, on each pedal stroke the Aluminum foil on the crank-arm contacts the two leads from the switches allowing current to flow, causing them to activate.

Example:

The cyclist is in the required test position and pedaling. The experimenter arms the switching circuit by closing switch S8. The next time the cyclist's left crank passes by the down tube, S1 is triggered and the LED system turns on. Once the cyclist's crank

reaches the seat tube, S2 is triggered and the LED system turns off. If by chance, the cyclist's crank activates switch S2 prior to activating switch S1, the process will continue as normal due to the relay S4. Thus, the only LED traces missing in the image of the pedal stroke will be in the angle between the down tube and seat tube. In the future, modifications can be performed to reduce the missing data by mounting the switches closer to each other. The attachment locations are shown below in Figure 9.

This automated switch system reduces the variation in the images captured. This switching circuit requires a minimal amount force to bring the two wires together, and thus dissipates a negligible amount of the cyclist's energy. With this system, the experimenter must simply press the trigger for each of the two cameras, and as soon as the cameras' shutters open, the switching circuit is armed and the cyclist's next pedal stroke will be captured as a series of LED flashes.

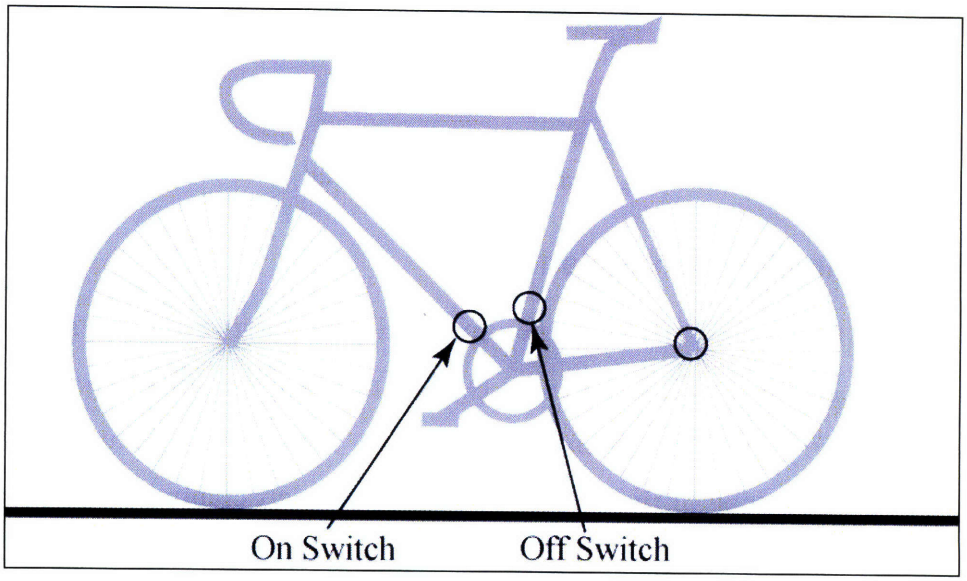

Figure 9: Attachment locations of the On and Off switches from the Switching Circuit

2.5 The Flashing Circuit

The output of the LED flashing circuit is an adjustable-frequency square wave with approximately 3V peak. The circuit is a standard oscillator circuit driven by a 555-timer IC [8]. The flashing frequency and the on-off switch is governed by the values of the resistors and capacitor in the circuit and is outlined below. The parallel array of LEDs are driven by the LED flashing circuit and supplied by 6V. The resistances in series with

the LEDs may need to be modified depending on the color associated with the LED. A picture is shown in Figure 10.

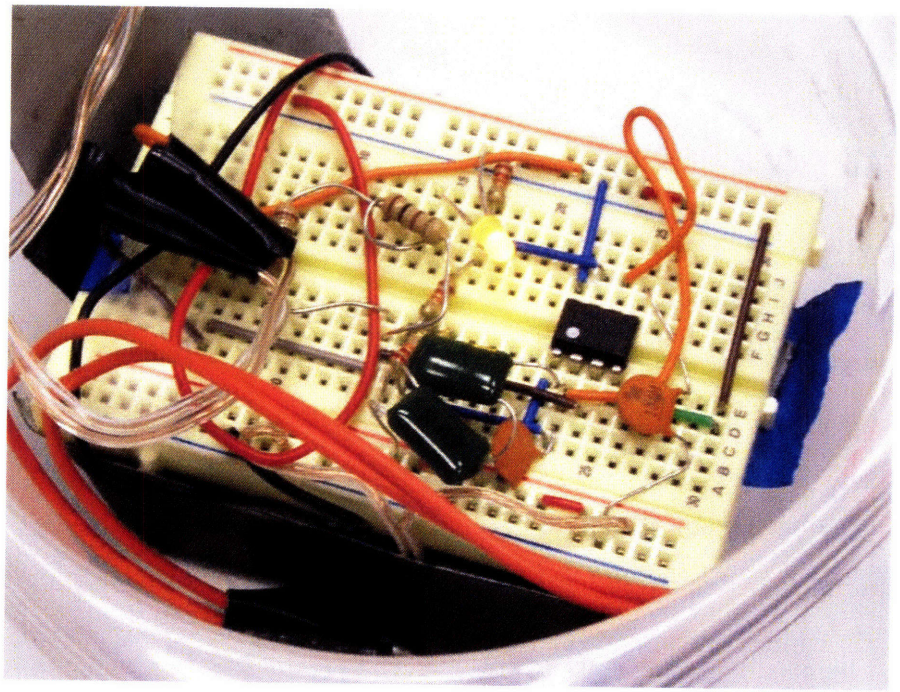

Figure 10: The LED Flashing Circuit. The yellow LED indicates that the circuit is on

2.5.1 Frequency, Time-On and Time-Off

The following relationships determine the frequency and on-off times of the flashing LEDs:

Time On (sec):

$$T_1 = 0.693(R_2 + R_3)C_2$$

Time Off (sec):

$$T_2 = 0.693R_3C_2$$

Frequency (Hz):

$$Frequency = \frac{1.44}{C_2(R_2 + R_3)}$$

The circuit used in this experiment had the values $R_2 = 22k\Omega$, $R_3 = 66k\Omega$, $C_1 = 0.1\mu F$, $C_1 = 0.194\mu F$. This gives $T_1 = 0.0118sec$, $T_2 = 0.0089sec$, **Frequency = 48.3Hz.** This is

close to the experimentally measured LED flashing frequency of 46Hz, found using the procedure in Appendix 12.1.2.

2.6 Cameras

Three standard off-the-shelf amateur digital cameras were used in this experiment. Most other types of digital cameras will also work as long as one can obtain an approximately two-second exposure time.

Camera 1: Olympus Camedia D580. This camera is a standard point and shoot camera. It was used in night mode which gave about a 2 second exposure time. This camera was mounted to the custom bicycle cable switch tripod, and was used to capture images of the cyclists' lateral area.

Camera 2: Olympus Stylus 770 SW. This camera is a standard point and shoot camera. This camera was used in night mode, which gave approximately 2 second exposure time. This camera was mounted on a tripod and was one of the two used to capture images of the LED traces.

Camera 3: Canon EOS Digital Rebel. This camera is a digital single lens reflex camera with a 17-40mm f4.5/5.6L lens. This camera was used with a 2.5 sec exposure time, set manually on the camera. This camera was mounted on a tripod and was one of the two used to capture images of the LED traces.

2.7 Camera Shutter Release and Camera Setup

Any movement of the cameras during the experiment dramatically reduces the accuracy of the 3D data and voids the calibration. Two systems were used in this experiment to allow the user to activate the cameras' shutters without manually pressing them. Electronic and mechanical shutter release cables were developed for each of the cameras to prevent human induced camera movement.

A custom cable release was built for the Canon Rebel camera. The cable release consisted of a 30ft cable connected to the camera via a 1.8mm stereo plug. The shutter is released when the photographer closes the circuit by pressing the shutter button. Since the Olympus Camedia lacked a plug for an electronic cable release, a mechanical cable

release was developed based on a brake cable concept and is shown in Figures 11 and 12 below. By pressing a brake lever on a pair of bicycle handlebars, a small wooden lever moved to press the camera's shutter button, resulting in a photograph being taken. In this way it was possible to take a photograph without moving the camera.

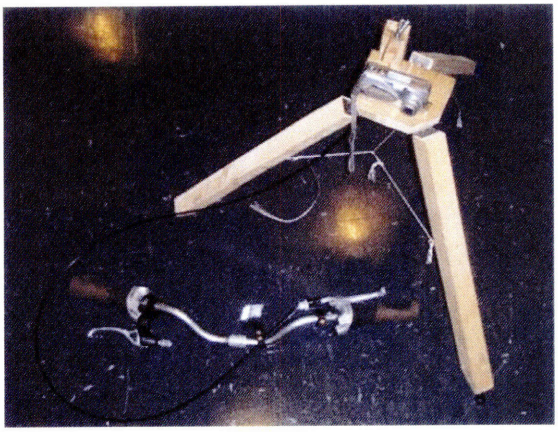

Figure 11: Camera setup showing cable switch. Pressing the brake lever on the bicycle handlebars presses the trigger on the camera, enabling the user to take pictures from as far as six feet away.

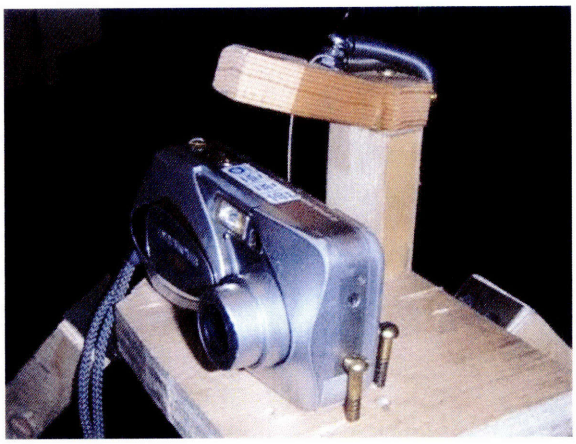

Figure 12: Close-up of the trigger lever, actuated by the bicycle brake lever. The camera is the Olympus Camedia D580.

2.8 Synchronizing Photos: Digital clock with seconds display

A digital clock with a seconds display was placed near the cyclist to generate a unique time signature on the photograph pairs. In addition, the internal clocks of each of the cameras were synchronized. Using this dual-synchronization, picture-pairs could easily be associated post-experiment.

2.9 Cycle trainer

A *Kinetic* fluid cycle trainer (Figure 13) was used to hold the bike upright and to provide the desired resistance to the back wheel. The *Kinetic* cycle trainer was chosen for its stability and operation smoothness at high speeds.

Figure 13: *Kinetic* fluid cycle trainer used in this experiment. Tightening the knob in the back increases the riding resistance

2.10 PowerTap wheel and computer

Power output was measured by a 700mm wheel with a PowerTap hub, made by the CycleOps company. The subject's cassette was removed and placed on the hub of the PowerTap wheel. A strain gauge sensor system inside the hub is used to measure the torque, which is subsequently transmitted wirelessly the frame-mounted sensor. The sensor can be attached to a computer or meter which displays power output and speed.

2.11 Calibration frame

In order to transform the two-dimensional stereo-photographs into three-dimensional data, a spatial calibration must be performed. The calibration is performed by photographing LEDs with known position in three-dimensional space. A 6ft high, 6ft long and 3ft wide PVC calibration frame was built to space LEDs by 1ft in all directions. To enable portability, each 6ft section consisted of two 3ft sections. The calibration frame and corresponding calibration image-pairs are shown in Figure 14 below.

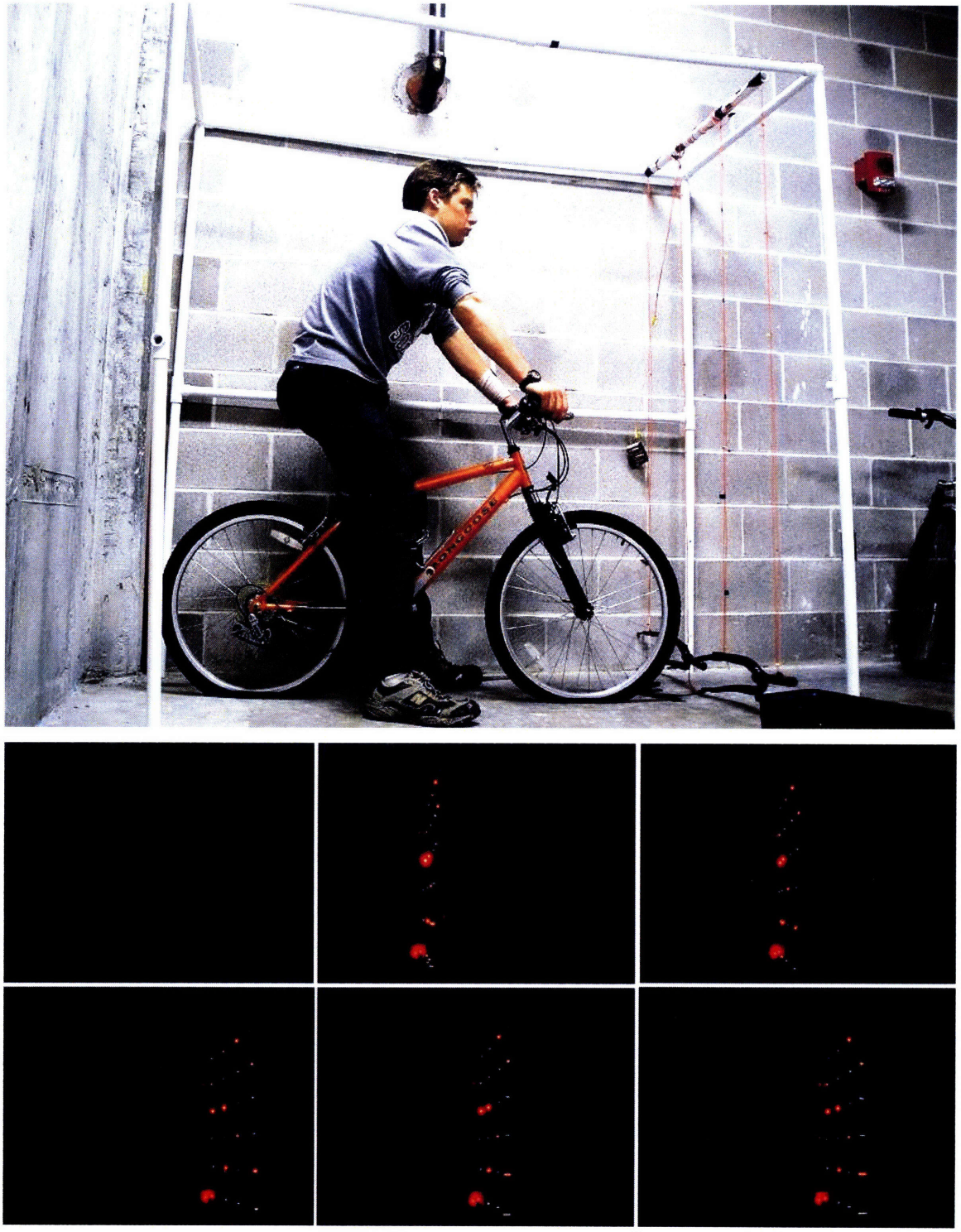

Figure 14: Calibration frame (top) with curtain of 24 LEDs on the right ride. The LED curtain was moved to each of the six positions and photographed for calibration (below)

A top view of the complete experimental setup is shown below in Figure 15

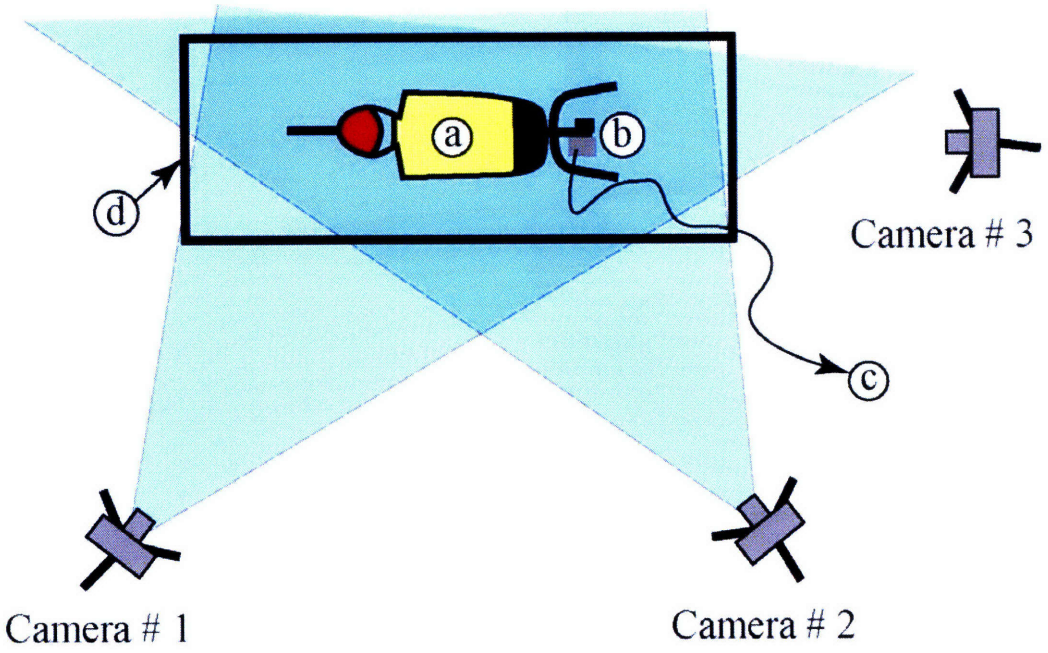

Figure 15: Top view of the experimental setup showing (a) the cyclist, (b) the cycle trainer, (c) the computer output from the PowerTap wheel showing speed and power, and (d) the calibration frame.

Chapter 3: Kinematics analysis tools

Although cycling motions are mostly planar, measuring three-dimensional joint locations enables quantification of the out of plane motion. In addition, since the motion capture system which is proposed in this thesis is intended to be applicable to general three-dimensional sports analysis, we present a three-dimensional reconstruction in the simpler case of cycling to demonstrate the effectiveness of the system.

3.1 Three Dimensional Data Reconstruction

When points are recorded in two or more different camera views (stereo-photogrammetry), it is possible to determine the three-dimensional coordinates of those points. The reconstruction of three-dimensional point locations is accomplished by creating a calibration which can be used to determine the rays associated with the point u,v-image coordinates.

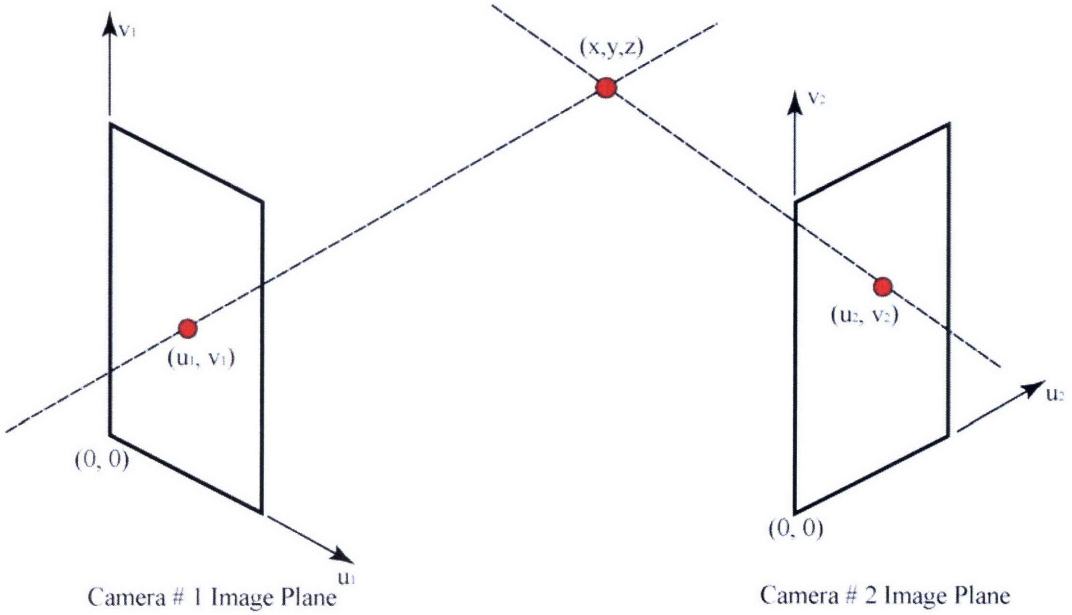

Figure 16: The intersection of light-rays illustrates the relationship between three-dimensional *x,y,z*-coordinates of a point, and the corresponding *u,v*-locations in the camera image planes. From this image it is clear that the location of a three-dimensional point can be determined from the intersection of image plane rays. The calibration process is used to determine the rays from the *u,v*-coordinates in the image plane.

3.2 Data Extraction and Reconstruction Using Matlab

The data extraction is performed using a custom Matlab code. This code has three main components:

1. Calibration of the three-dimensional space
2. Data Extraction from two-dimensional images
3. Conversion of the two-dimensional data to three dimensional coordinates

3.2.1 Calibrating the three dimensional space

The direct linear transformation (DLT) [9,10] is used to provide the functional relationship between the two-dimensional *u,v*-image-coordinates and the three-dimensional *x,y,z*-space. To determine the DLT coefficients, a series of points with known three-dimensional coordinates must appear in the photographs. In the calibration process, the relative positions of the LEDs hanging from the calibration frame are known

in three-dimensional space and act as the known coordinates. The calibration process uses the known three-dimensional coordinates and their respective locations in the images to determine DLT coefficients. These coefficients contain the necessary information to determine the camera position as well as the rays associated with the *u,v*-image coordinates. For each point in the calibration image, the following two equations can be written and compiled into an overall system of equations for the calibration:

$$\begin{bmatrix} u \\ v \end{bmatrix} = \begin{bmatrix} x & y & z & 1 & 0 & 0 & 0 & 0 & -ux & -uy & -uz & \xi r^2 R & \xi r^4 R & \xi r^6 R \\ 0 & 0 & 0 & 0 & x & y & z & 1 & -vx & -vy & -vz & \eta r^2 R & \eta r^4 R & \eta r^6 R \end{bmatrix} \begin{bmatrix} L_1 \\ L_2 \\ L_3 \\ L_4 \\ L_5 \\ L_6 \\ L_7 \\ L_8 \\ L_9 \\ L_{10} \\ L_{11} \\ L_{12} \\ L_{13} \\ L_{14} \end{bmatrix}$$

$$R = L_9 x + L_{10} y + L_{11} z + 1$$

$$[\xi, \eta] = [u - u_o, v - v_o]$$

$$r^2 = \xi^2 + \eta^2$$

The first eleven DLT coefficients (L_1 – L_{11}) define a linear relationship between the known *x,y,z*-coordinates and the *u,v*-image coordinate registered in the camera image planes during the calibration process. The remaining DLT coefficients (L_{12} – L_{14}) are included to account for optical distortion and lens shift.

3.2.2 Data Extraction from two-dimensional images

We extract image coordinates from the two-dimensional photographic images using a custom developed Matlab (Mathworks, Natick, MA) code. Using Matlab's built-in image manipulation routines, the individual images are loaded into a series of matrices which represent the intensity of the red, green and blue color components of the image.

After the images are loaded, an averaging/smoothing filter is applied to the image in order to reduce any noise in the image.

The extraction of the location of the LED flash traces is performed in a semi-automatic manner. To initialize the LED flash tracking, the first three LED flashes are manually located and the coordinates of the centroids of the high-light-intensity regions are recorded. Following this, the remaining the LED locations are determined using an extrapolation based on the locations of the previously recorded LED flashes. This extrapolation is based on an over-constrained cubic polynomial fit of the LED trace. The extrapolation of subsequent points is user monitored to ensure data robustness. Following the extrapolation of the new LED flash location, the centroid of the nearest high intensity photographic recording is found.

3.2.3 Conversion of two-dimensional data to three-dimensional coordinates

The two-dimensional data is converted to three-dimensional data using the direct linear transform calibration coefficients computed during the calibration phase. This part of the process uses the DLT coefficients to relate the *u,v*-image coordinates to the corresponding rays which, when they intersect give *x,y,z*-coordinates. In practice, the rays may not exactly intersect; however, since a least squares solution method is used to determine the *x,y,z*-coordinates, the nearest location to an intersection is found. Since a least squares procedure is used, the addition of more camera views further enhances the three-dimensional reconstruction accuracy. To determine the *x,y,z*- location of each point which appears in two or more camera images, the following two equations can be written for each camera, resulting in a over-constrained linear system of equations:

$$\begin{bmatrix} \nu L_9 - L_1 & \nu L_{10} - L_2 & \nu L_{11} - L_3 \\ \omega L_9 - L_5 & \omega L_{10} - L_6 & \omega L_{11} - L_7 \end{bmatrix} \begin{bmatrix} x \\ y \\ z \end{bmatrix} \begin{bmatrix} L_4 - \nu \\ L_8 - \omega \end{bmatrix}$$

$$[\nu, \omega] = [u - \xi(L_{12}r^2 + L_{13}r^4 + L_{14}r^6), v - \eta(L_{12}r^2 + L_{13}r^4 + L_{14}r^6)]$$

Chapter 4: Aerodynamics Analysis

In order gain insight into a cyclist's choice of a riding position, our measurement of cyclist kinematics and power is supplemented with aerodynamics considerations. To examine the aerodynamics of cycling two subjects were selected to test in the Wright Brothers Closed Return wind-tunnel on the MIT campus. Knowing the cyclist's drag at each position can provide indications of the power lost due to air resistance. Due to limited access to the wind tunnel facility a small number of subjects were tested in the wind-tunnel in order to determine drag coefficients (C_d) for each cyclist position:

$$F_d = 0.5 C_d \rho V^2 A_f \qquad (1)$$

where F_d is the drag force, ρ is the density of the air, V is the windspeed, and A_f is the rider's frontal area. The drag force on the cyclist and bike is measured using a six degree of freedom balance onto which a custom bike stand is mounted. A schematic of the Wind Tunnel setup is shown in Figure 17 and a photo of the setup is shown in Figure 18.

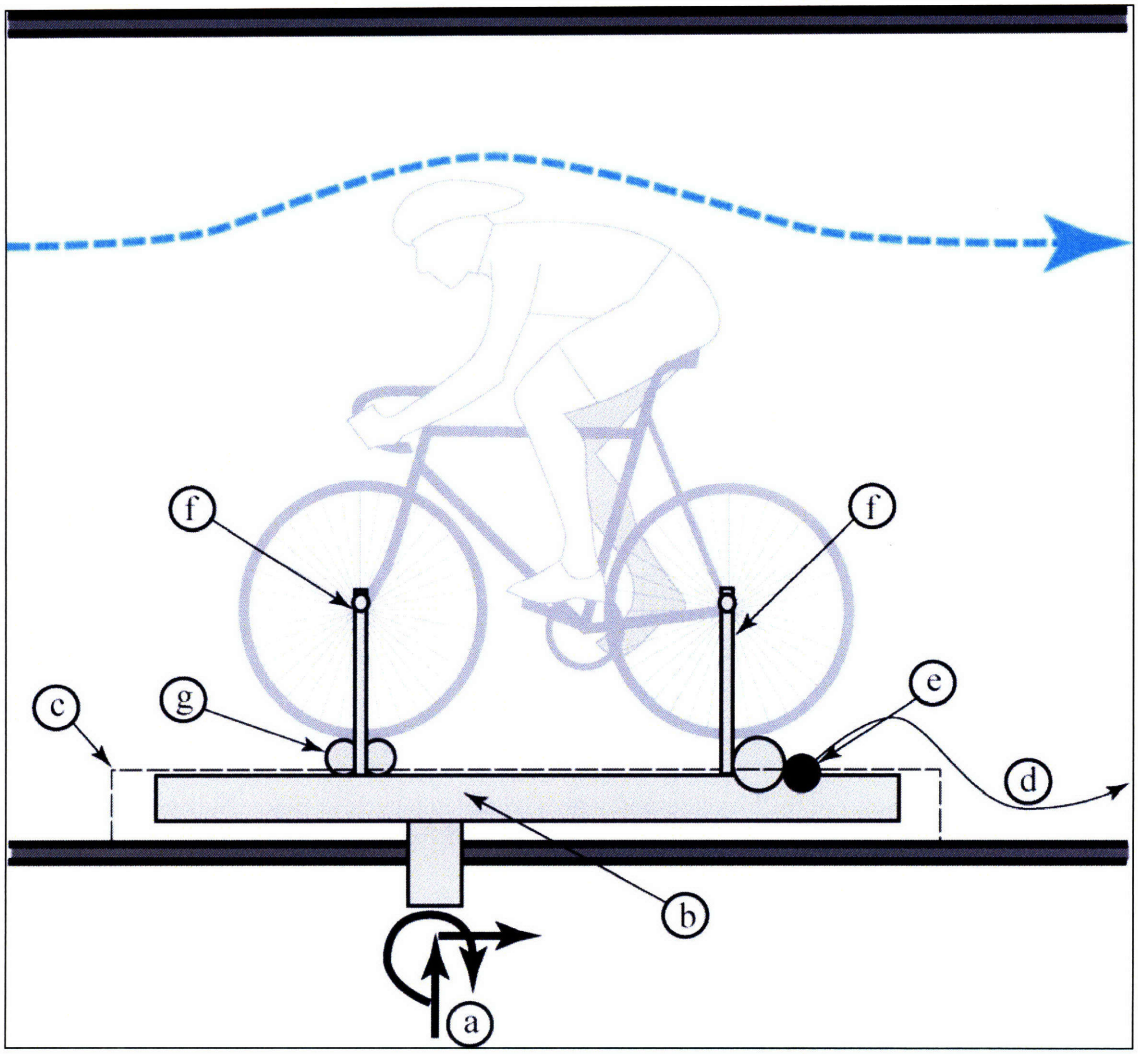

Figure 17: Schematic showing wind tunnel setup. Wind flows at the rider from right to left. The bike is mounted on the stand (b) at the axles (f). The front wheel is positioned between two free rollers (g), while the back wheel is positioned over the CycleOps power meter wheel (e). The distance between (g) and (e) can be varied to accommodate differently-sized bikes. The output from the power meter is sent via wire (d) to a computer. The aerodynamic drag force of the cyclist is measured by six strain gauges mounted to the base of the stand at (a). A wooden skirt (c) is placed around the base of the stand to prevent additional drag.

Figure 18: An illustration of the bicycle stand with a triathlon bicycle in place. Notice the skirt which is placed around the bicycle stand to prevent the bike stand from generating additional drag to the system.

4.1 Frontal Area A_f

The cyclist's frontal area was determined from photographs taken a certain distance behind each of the subjects. The number of pixels representing the frontal area of the subject was determined using a custom Matlab code. To determine the area represented by each of the pixels, the camera's field of view in both the horizontal and vertical directions is needed. To calibrate the pixel area, the Olympus Camedia was positioned in front of an object of known width. The camera was positioned so that the object completely occupied the field of the camera. The horizontal angular field of view was found to be 53.3 degrees with a vertical angular field of 39.5 degrees.

In order to find the subject's frontal area, the Olympus Camedia was placed at a known distance away from the subject designated r, typically between 80 and 100 inches. At this distance r, the effective "area" A_{total} captured by a picture is determined using the formula

$$A_{total} = 4r^2 \tan\left(\frac{\alpha}{2}\right)\tan\left(\frac{\beta}{2}\right) \qquad (2)$$

where α is the horizontal angular field of view of the camera (53.3 degrees in this case) and β is the vertical angular field of view of the camera (39.5 degrees). Thus, the raw frontal area of the subject A_s is given by

$$\frac{P_s}{P_{total}} = \frac{A_s}{A_{total}} \tag{3}$$

where P_s is the number of pixels taken up by the cyclist in the image, and P_{total} is the total number of pixels in the image (2288 X 1712 in this case). In each of the frontal area pictures the camera was positioned so that the subject was in the middle of the frame, to reduce any distortion at the edges of the image.

A Matlab program was created to determine P_s for each cyclist. The program prompts the user to load the picture of the cyclist in the desired position, then click points on the outside of the cyclist's body to generate a bounding polygon (see Figure 19). The program then calculates the number of pixels enclosed within the bounding polygon. From Equations (2) and (3) the raw frontal area of the cyclist can be computed as a function of r.

Throughout the cyclist's pedal stroke, his/her frontal area changes as the legs change position. In order to compute an average drag, the frontal area corresponding to the portion of the body above the center of the crankarm is considered.

It was found that this formula produced a consistent underestimate of the actual frontal area of the cyclist. This inaccuracy was attributed in part to camera distortions around the edges. In order generate a correction to this under-prediction of area, objects of known size were placed at known distances from the camera and photographed. The Matlab program was then used to calculate the object's raw frontal area A_s. The objects used (a 27" diameter circle and a 18.25" X 39.5" rectangle), were both similar length scales as the cyclists. The objects were placed in a plane parallel to the camera's lens at distances between 60" and 120". The computed frontal areas were a factor of 0.76 to 0.83 less than the actual frontal areas. For a distance of 100" and an object of known size, most closely approximating the size of a cyclist, the correction factor was approximately to 0.8. Thus, a correction factor of 1/0.8 = 1.25 was used in subsequent calculations to better estimate the actual frontal area A_f of the cyclist. In future work it will be necessary to develop a more rigorous formula to find the cyclist's frontal area that more accurately

takes into account camera distortion. In addition, it would be helpful to replace the single calibration object with an area calibration grid of known dimensions in the camera's field of view. This would allow a more accurate calculation of the area associated with each pixel.

4.2 Drag coefficient C_d

Given the frontal area A_f of the cyclist using the Matlab program and from wind tunnel data for the drag force F_d, the coefficient of drag C_d can be determined for each of the wind tunnel subjects using Equation (1) This position-specific drag coefficient is used to compute the approximate drag of other cyclists in similar body positions who were not analyzed in the wind tunnel.

Figure 19: Using the frontal area Matlab program to calculate the frontal area of a Mountain Biker. The yellow polygon tracing the perimeter of the subject is clicked manually.

4.3 Optimal cycling positions

By combining power and aerodynamics considerations insight is gained into which cycling positions are most appropriate for hill climbing. It is assumed that a cyclist can attain speeds less than 20m/s for a given power output, simply by shifting gears (wheel friction within the wheel bearings is assumed to be negligible for this analysis). From the drag coefficients the expected drag forces on each subject based on their speed can be calculated. The power lost to drag P_{drag} is found by multiplying the drag force (Eqn (1) above) by the velocity V to obtain

$$P_{drag} = \frac{1}{2} C_d \rho V^3 A_f \tag{4}$$

The power approximations can be extended to include power lost while climbing a hill of angle θ, P_{hill}, which is given by

$$P_{hill} = mgV \sin(\theta) \tag{5}$$

from trigonometry, where m is the mass of the cyclist and g = 9.8m/s^2. By subtracting the power lost due to drag and to hill climbing from the power generated P_G by the cyclist, a formula for the "excess" power available to the cyclist, P_{excess}, can be approximated by:

$$P_{excess} = P_G - \frac{1}{2} C_d \rho V^3 A_f - mgV \sin(\theta) \tag{6}$$

From this equation the excess power available to a cyclist can be predicted. Each cycling position has a different frontal area, and thus different associated C_d, thus excess power vs speed curves for a variety of different positions can be computed. From Eqn (6) it is hypothesized that at lower speeds the most power-efficient cycling positions will have the most "excess" power, and will thus be optimal. Conversely, at high speeds aerodynamic drag effects will dominate and the most aerodynamic positions will be optimal. By constructing and examining these excess power vs speed curves predictions can be made to indicate which positions are power-optimal over a range of speeds.

Chapter 5: Cycling Kinematics

Measuring the kinematics of cyclists is demonstrated as an initial application of the proposed motion capture system.

5.1 Positions and exertion levels tested in this experiment

Five standard cycling positions are analyzed (see Figure 20):

1. Upright "tops" position (A)
2. Hoods position (B)
3. Drops position (C)
4. Standing position (D)
5. Drops & aero position (E).
6.

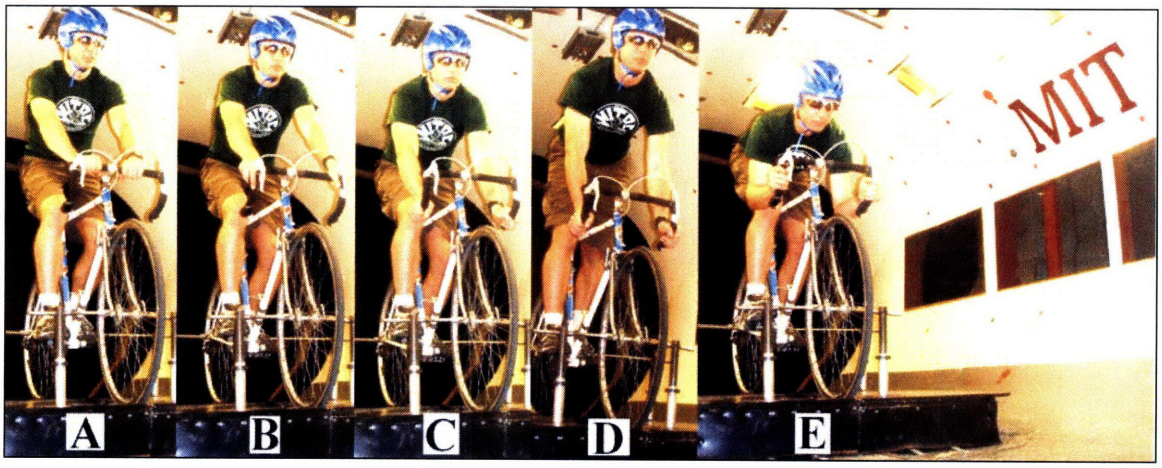

Figure 20: Five cycling positions tested in this experiment: tops (A), hoods (B), drops (C), standing (D), aero (E). Photographs were taken in the MIT Wind Tunnel.

In order to find a correlation between cycling kinematics and power output kinematics at both a low and a high exertion level were studied. For the low exertion level, subjects were asked to cycle at an exertion level corresponding to that of a casual twenty-mile "Sunday afternoon ride." For the high exertion level, subjects were asked to pedal at a speed corresponding to a twenty-mile race pace. The different cycling positions and exertion levels tested for the road bikes in this experiment are shown in Table 1.

Scenario #	Position	Exertion Level	Comments
1	A	Low	
2	B	Low	
3	C	Low	
4	A	High	
5	B	High	
6	C	High	
7	D	Low	Only if comfortable. Not in Wind Tunnel
8	E	Low	Only if comfortable. Not in Wind Tunnel

Table 1: The different position and exertion level scenarios tested in this experiment

The kinematics associated with mountain biking were investigated for two subjects. The two positions tested were (A) seated and (B) standing, shown in Figure 21. The positions investigated for the triathlon bike are shown in Figure 22. These positions correspond to (A) Tops, (B) Horns/Drops and (C) Aero/Aerobars.

Figure 21: Mountain biking positions tested in this experiment: (A) seated, (B) standing

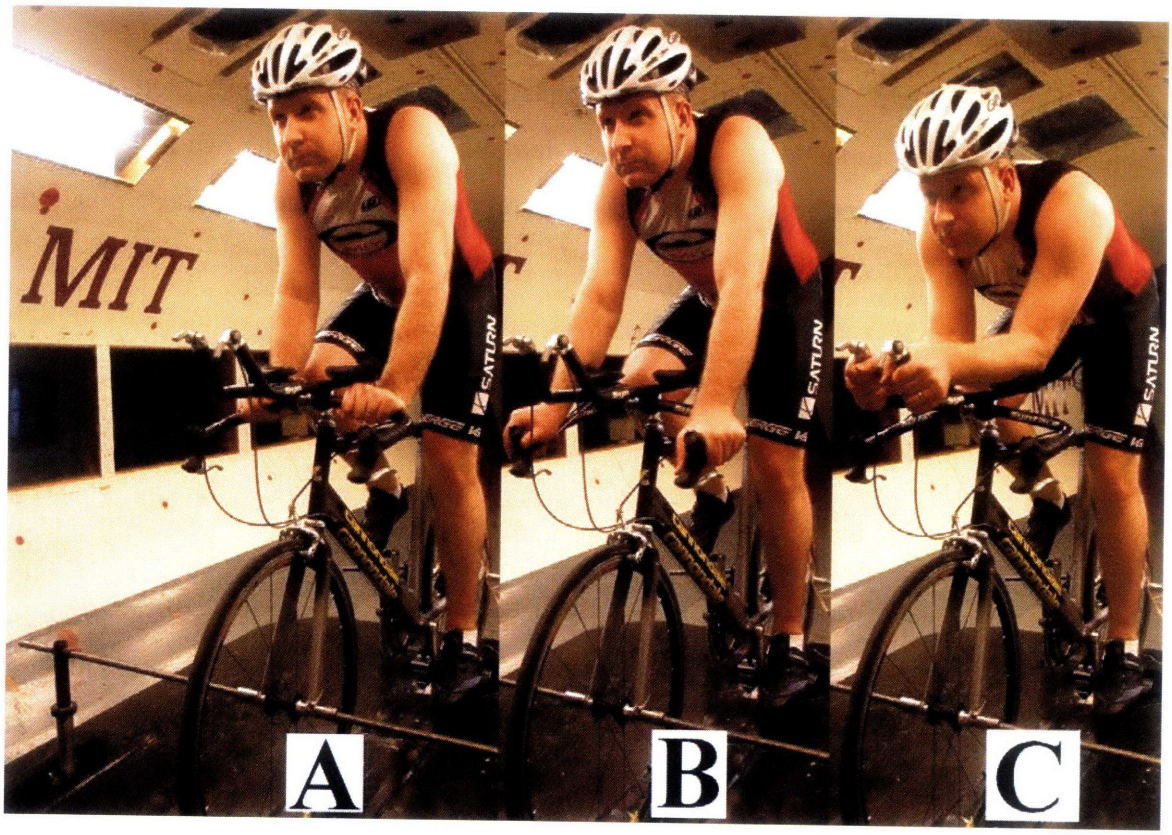

Figure 22: Triathlon cycling positions: (A) tops, (B) drops/horns, (C) aerobars

In the experiment subject-to-subject kinematics variations as well as body kinematics to power output relationships are examined. This combined measurement of kinematics, power output and drag provides a framework for determining appropriate positions for different cycling situations (hill climbing, track racing, down-hill).

In order to measure the kinematics of the body, the motions of five major joints are measured: the shoulder, hip, knee, ankle, and toe. An intermediate LED is placed at the calf and thigh to allow us to track the joint motions with greater accuracy (see Figure 23).

Figure 23: LED locations and colors

Chapter 6: Procedure

Before the subjects arrived, the cameras, calibration frame, and cycle trainer were setup. All subjects were males, between 20 and 30 years of age. Every subject said they cycled for an average of five times per week. Each subject was briefed about the experiment and asked to read and sign a consent form prior to the experiment. Each subject was given a copy of their signed consent form and given a unique identifier code to maintain confidentiality. Each subject participated in this study one-at-a-time.

The following setup procedure was followed in preparation for data collection:

1) The bicycle cassette was installed on the power tap wheel
2) The bicycle was mounted onto the cycle trainer
3) The switch system and PowerTap receiver was attached to the bike
4) The LEDs were attached to the subject according to the map in Figure 2

The subject was asked to pedal in each scenario outlined in Table 1. As they pedaled at a constant rate, one experimenter recorded power and speed data from the PowerTap computer. In the meantime, the other experimenter captured two to three image pairs. The cyclist pedaled in each scenario for approximately 45 seconds, and was given the option of a 30 second rest in between scenarios. After kinematics were recorded a frontal area photograph was taken for each of the representative cycling positions.

After the experiment, the subject's bike was taken off the cycle trainer. The subject was asked if any of the positions felt unnatural, or particularly uncomfortable. The subject's total cycling time for the experiment was five to ten minutes. The subject was compensated with his choice of an energy bar. The total experiment time, including pre-experiment questions and LED placement, experiment and take down, for each of the cyclists was about forty minutes.

Prior to the data collection for each cyclist, the three dimensional space was calibrated, using the calibration procedure described in Appendix (12.1.3).

Chapter 7: Results and discussion

Approximately 800 images were gathered during the experiment. Shown below in Figure 24 are a series of sample images gathered by each of the two cameras for a cyclist on a triathlon bike.

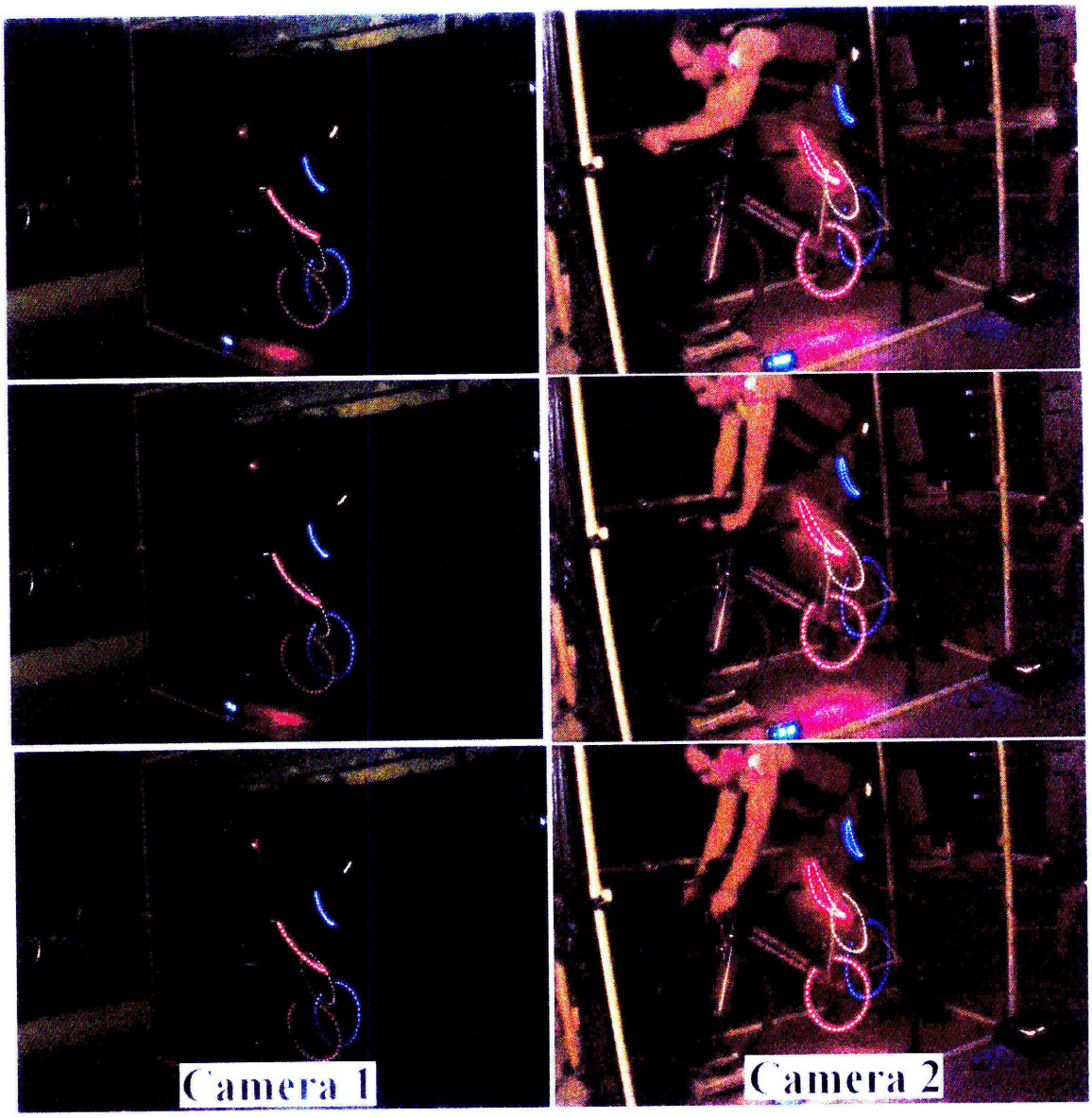

Figure 24: Typical images captured in the experiment by Cameras 1 and 2. The cyclist is pedaling in the aero-position in the upper pair of pictures, the tops position for the middle pair, and the drops position for the lower pair.

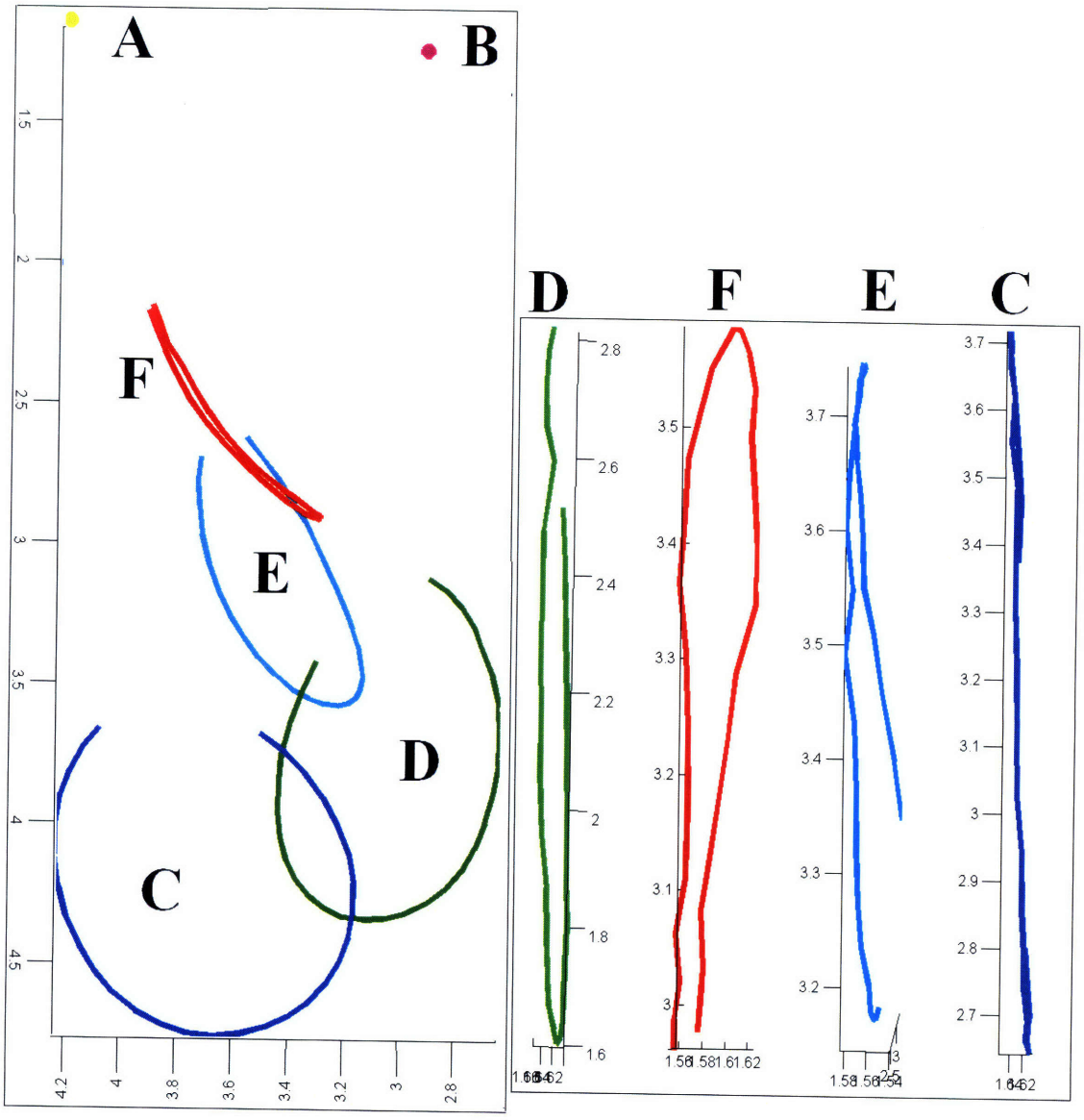

Figure 25: A side view of the 3D dimensional reconstruction (left) for a cyclist pedaling in the aero position, and an edge-on view of the LED traces from the front of the bike (right). (A) is the shoulder, (B) is the hip, (C) is the toe, (D) is the ankle, (E) is the shin, and (F) is the knee. The scales are in feet and are all 1:1.

The edge-view of the joints shows that all of the joints execute a slight excursion from the plane throughout the pedal stroke; the greatest out-of-plane excursion for this set of data occurs at the knee, with a deviation of approximately 0.95" during the pedal stroke. This shows that cycling motions are not confined strictly to the 2-D plane as originally expected.

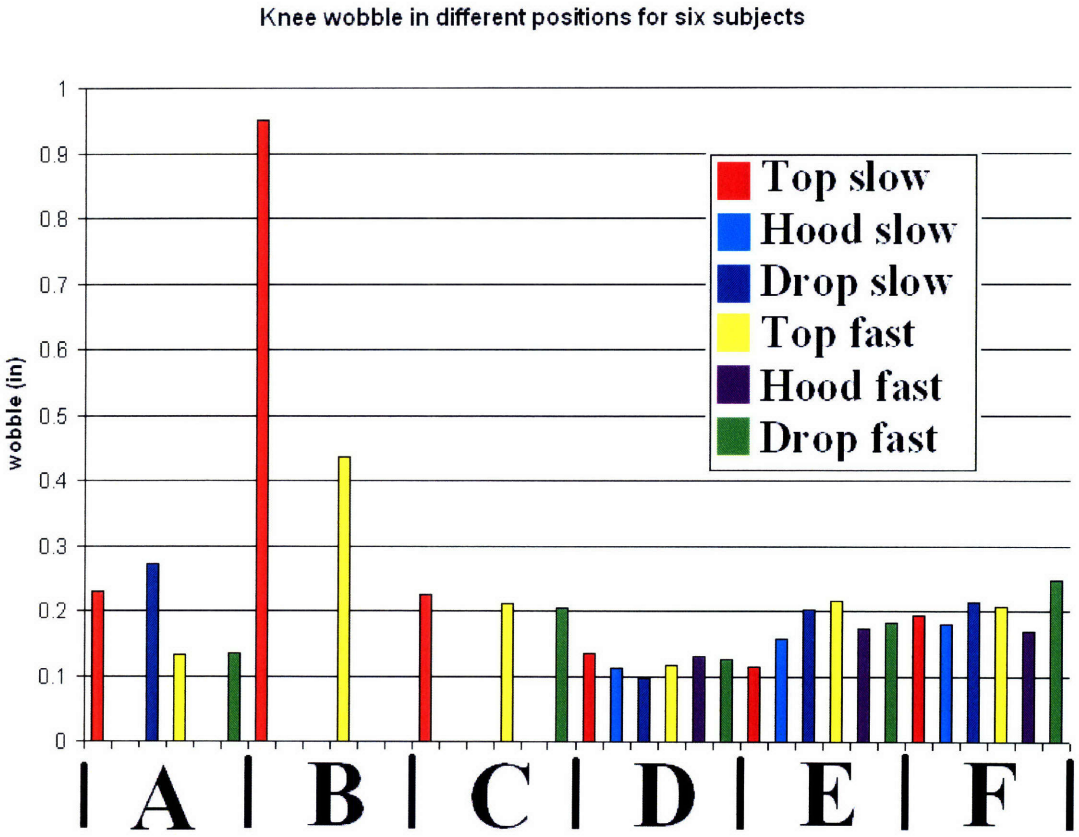

Figure 26: Range of movement of the knee in the out-of-plane direction (normal to the surface of the cyclist's bike) for six cyclists.

The data illustrates that the out of plane knee excursions are not negligible (Figure 26). The average out of plane knee excursion for the subjects was between 0.15 and 0.22 inches, with one subject demonstrating a much higher excursion (0.95in). Comparing across different positions, the average wobble in the tops positions was greatest (0.22in for tops fast), while the position with least wobble was the hoods position (0.15in for hoods slow). Future work would involve looking at the correlation between knee excursion, power output and susceptibility to injury.

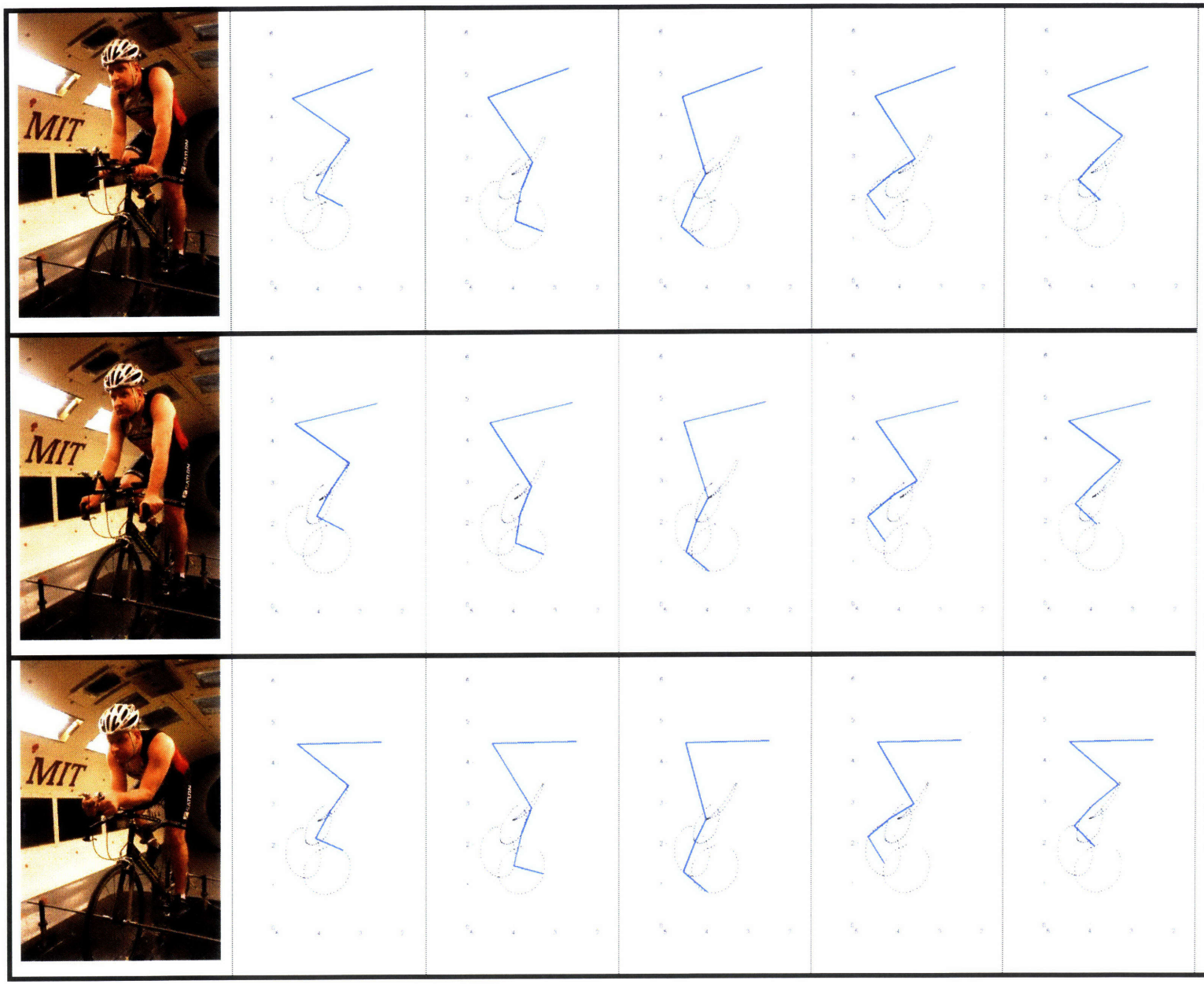

Figure 27: The characteristic triathlon cycling positions (top) horn-tops (middle) horns/drops (bottom) aero/aerobars. The extracted three-dimensional data is shown at 1/5 cycle increments from the side view for each position. The traces of the joints are shown with the discrete black dots while the instantaneous bone/joint positions are shown with blue lines.

Figure 28: The characteristic road-racing cycling positions (top) tops (middle) hoods (bottom) drops. The extracted three-dimensional data is shown at 1/5 cycle increments from the side view for each position. The traces of the joints are shown with the discrete black dots while the instantaneous bone/joint positions are shown with blue lines.

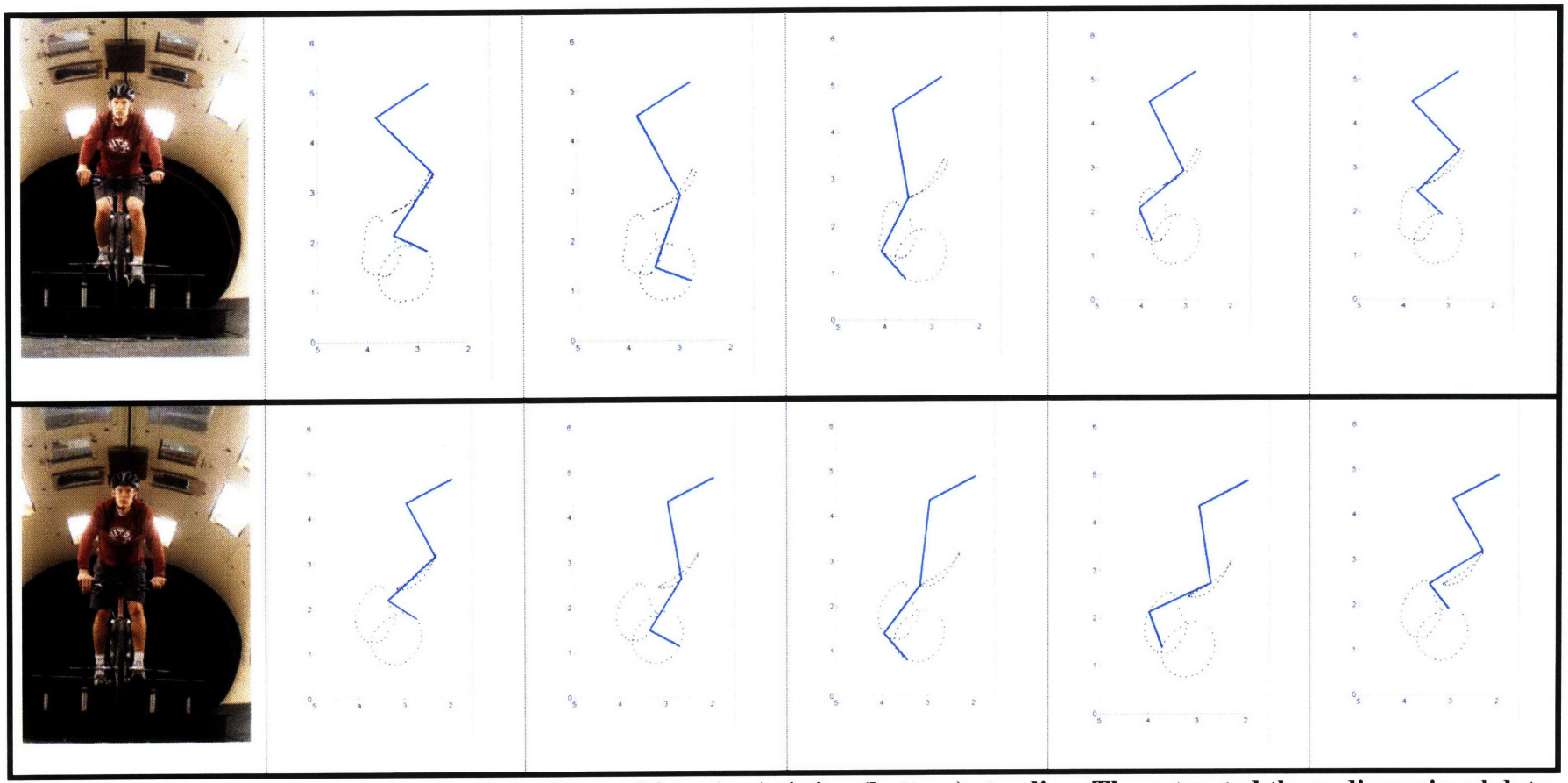

Figure 29: The characteristic mountain biking positions (top) sitting (bottom) standing. The extracted three-dimensional data is shown at 1/5 cycle increments from the side view for each position. The traces of the joints are shown with the discrete black dots while the instantaneous bone/joint positions are shown with blue lines.

7.1 Average power output

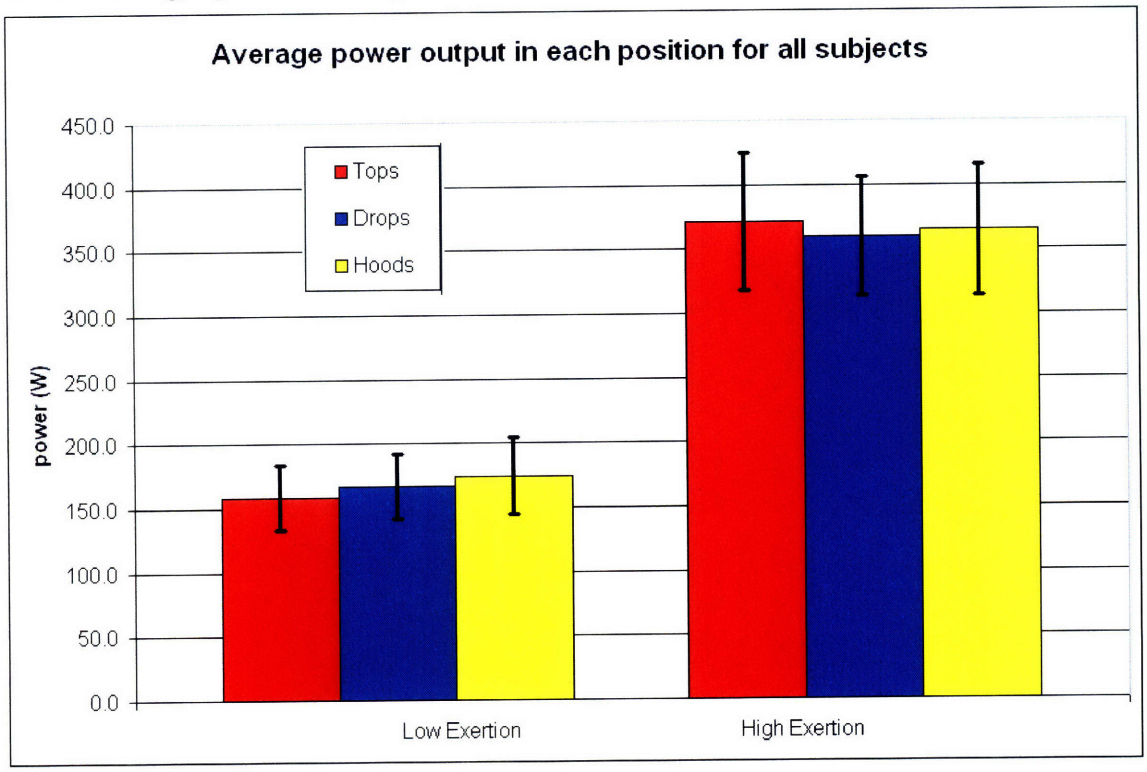

Figure 30: Power output averaged over eleven subjects at low and high exertion for tops, hoods, and drops positions.

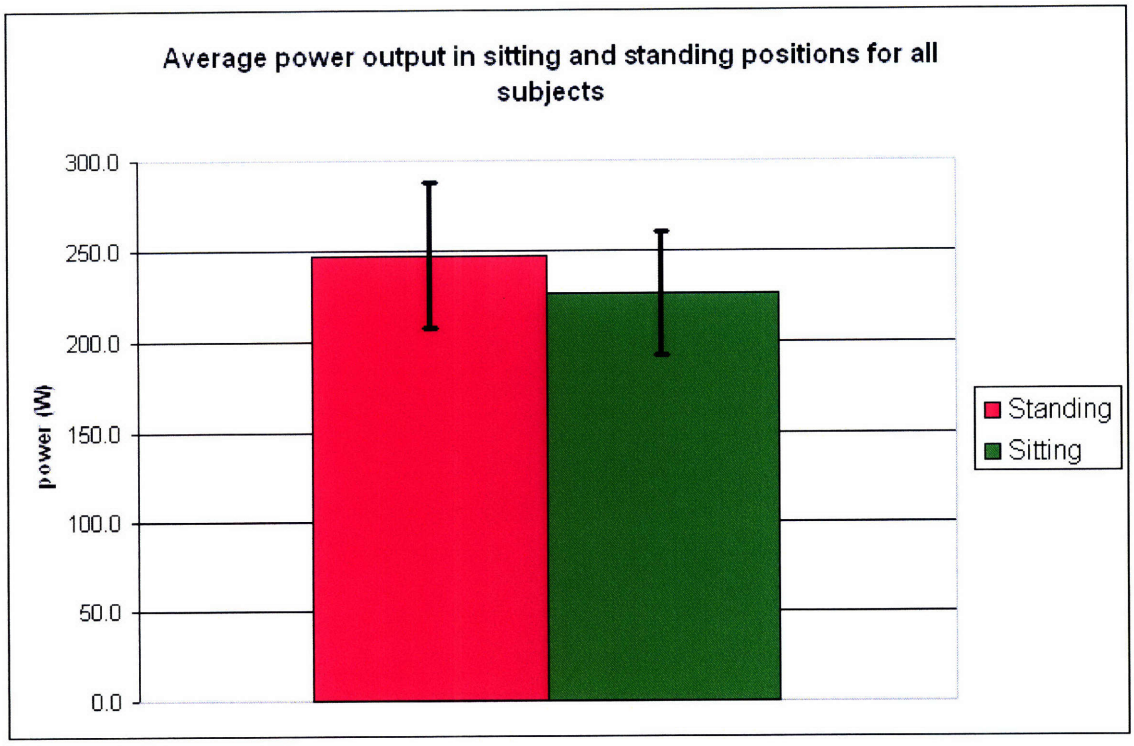

Figure 31: Power output averaged over eleven subjects in the standing and sitting positions

Figure 31 shows that the power output is greater in the standing position than in the sitting positions (averages for tops, drops, and hoods positions).

7.2 Joint angles versus time

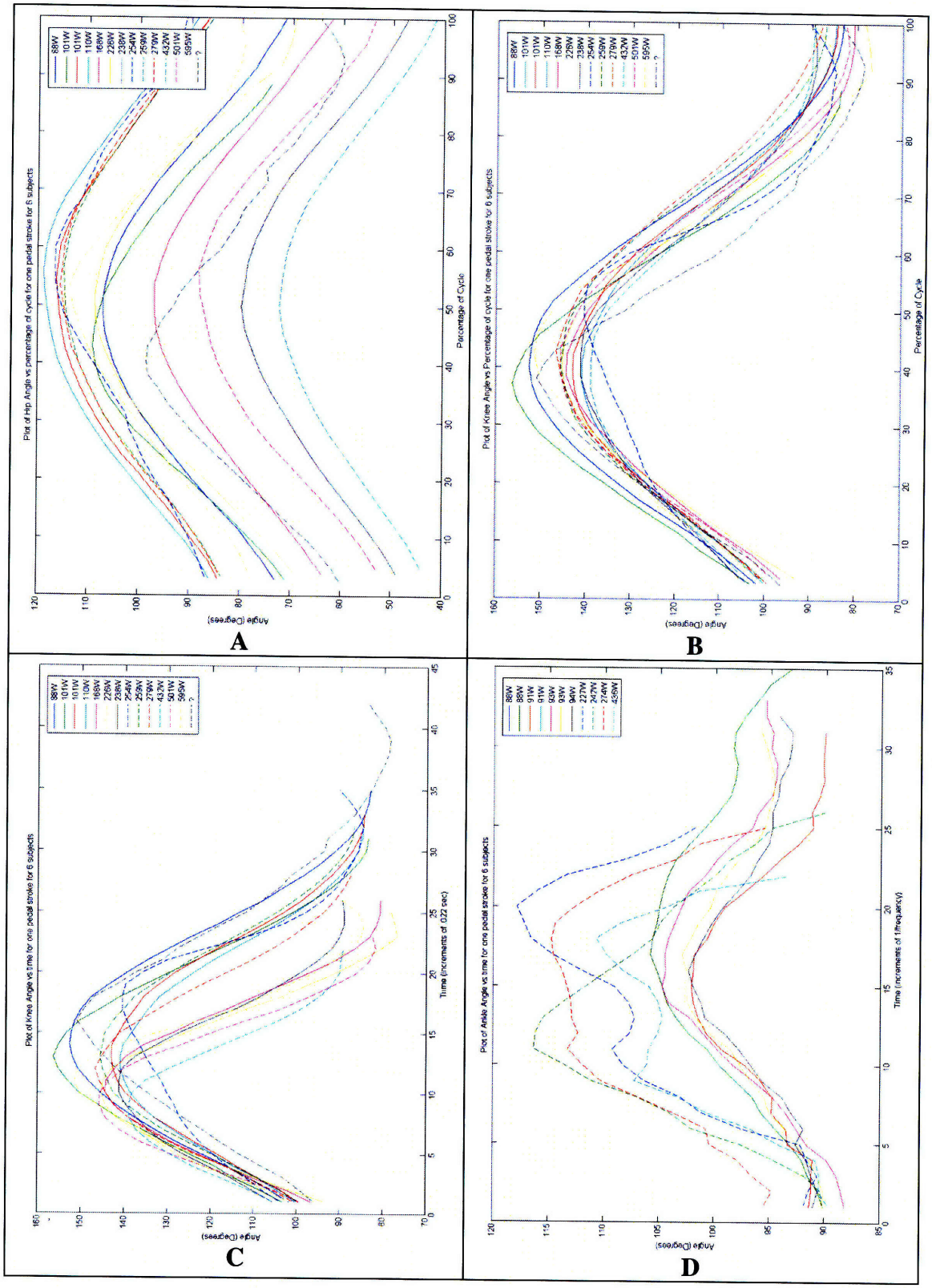

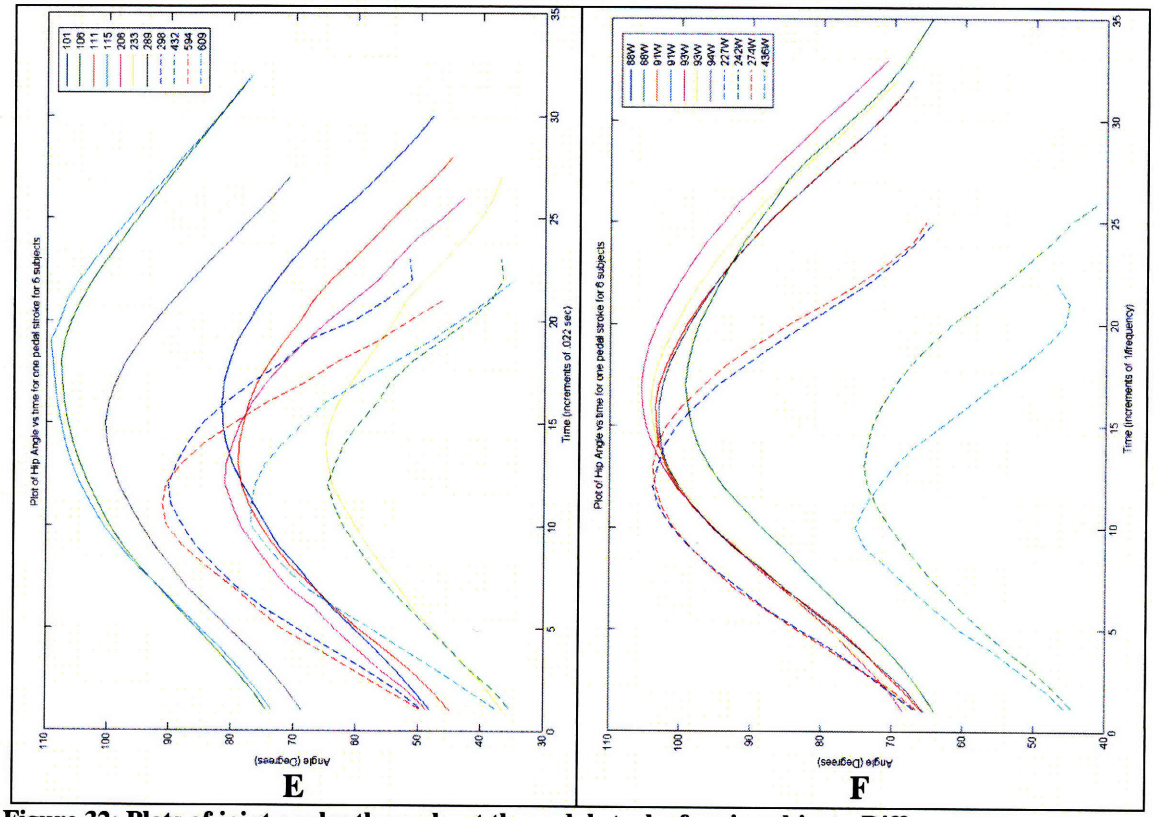

Figure 32: Plots of joint angles throughout the pedal stroke for six subjects. Different curves are different power outputs. Figure (A) shows tops position, (B) tops, (C) tops, (D) hoods, (E) drops, (F) hoods. (A) and (B) are plotted against % of pedal stroke completed, while the rest are plotted against time.

Figures 32A & B demonstrate the variability in two different angles between subjects. Figure 32A shows a 50 degree range of hip angles while Figure 32B shows a knee angle range of only about 20 degrees between subjects at different exertion levels. Figures E and F slow slight correlations between ankle angle and power output. In E and F the subjects with lower hip angles generally produced more power. It will be necessary to perform future analyses to gain deeper insight into this possible correlation.

The interesting dual peaks of several of the ankle angle traces in Figure 32D suggest two possibilities. This could mean that during the pedal stroke the ankle exhibits a more complex motion that expected, with a brief decrease in angle during the middle of the cycle. Or, it could highlight the difficulty in measuring ankle angle; small movements of the toe and ankle LEDs during the pedal stroke translate into dramatic changes in ankle angle, due to the relatively short distance from these LEDs to the ankle joint. In either case, higher ankle angles in D generally correspond to higher power outputs. In the future implementation of such a system, securing these LEDs to the subjects' toe and

ankle more firmly will be pursued. In addition, an examination of shorter LED flashed will be examined to determine if a more accurate digitization of the data is possible.

7.3 Power output versus joint angles

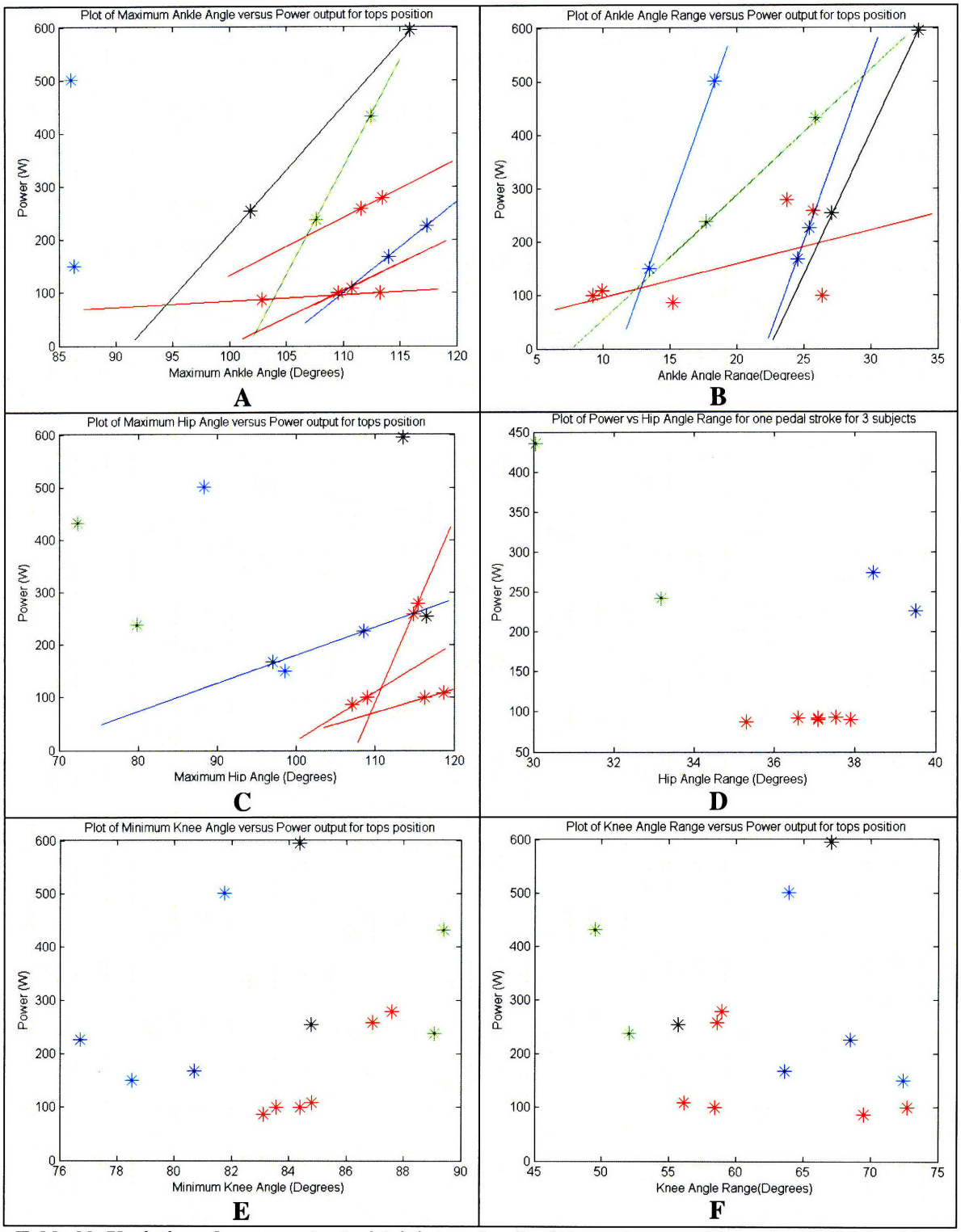

Table 33: Variation of power output with joint angles, for (A) maximum ankle angle, (B) total ankle angle range, (C) maximum hip angle, (D) total hip angle range, (E) minimum knee angle, and (F) total knee angle range. Same colors indicate the same subject.

Figures 33A & B show a slight positive correlation between ankle angle and power output. I.e., greater ankle angle ranges and higher maximum values generally correlate to higher power output. Figures 33E & F suggest that power output is not as strongly dependent upon knee angle. From the initial assumption of a five bar linkage, it is clear that the ankle angle possesses the largest potential for variation with exertion level. This positive correlation indicates that there may be several physiological suggestions related to ankle actuation strength and flexibility to promote power output increases. Further experiments and analysis should be performed to confirm this analysis.

7.4 Cycling position transition points

In order to find the optimal cycling positions at each speed, as described in Section 4.3, it is first necessary to find the drag coefficients C_d. The frontal areas for a representative subject were measured using the custom Matlab code, and using wind tunnel data and Equation (1) the C_d's were calculated, and they are shown in Table 2.

Position	Cd
Stand	1.33
Tops	1.26
Hoods	1.21
Drops	1.17
Aero	1.10

Table 2: drag coefficients for one subject

These drag coefficients were combined with Equation (6) to generate power vs speed curves which include aerodynamic power losses, cyclist power and grade-climbing power for a variety of different positions and hill angles, some of which are shown below.

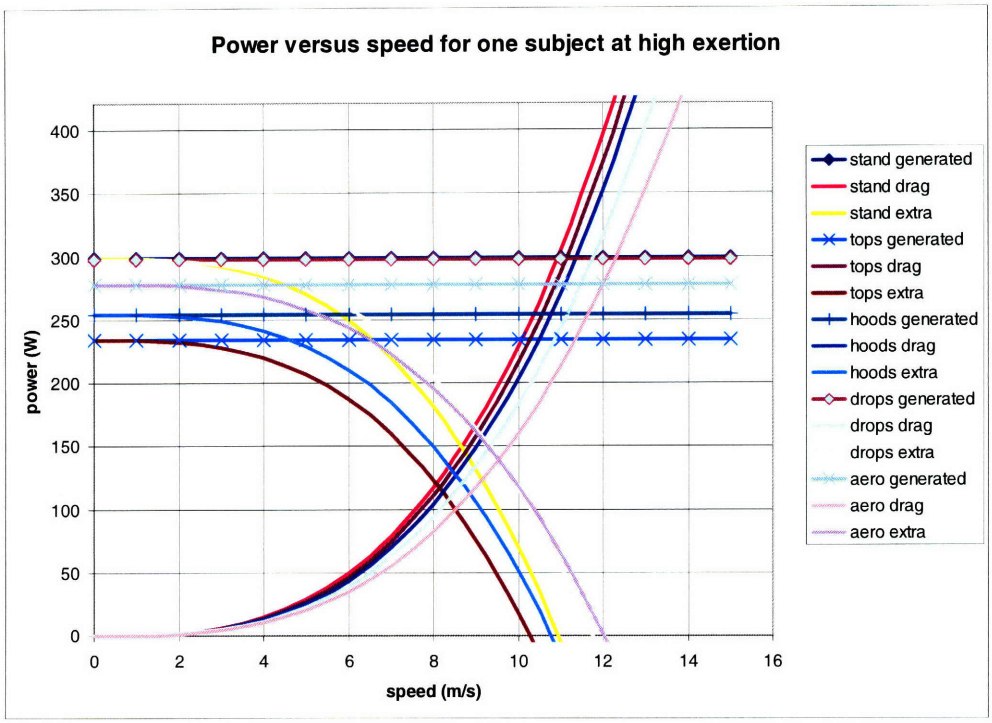

Figure 34: Predicted power vs speed curves for one subject at high exertion

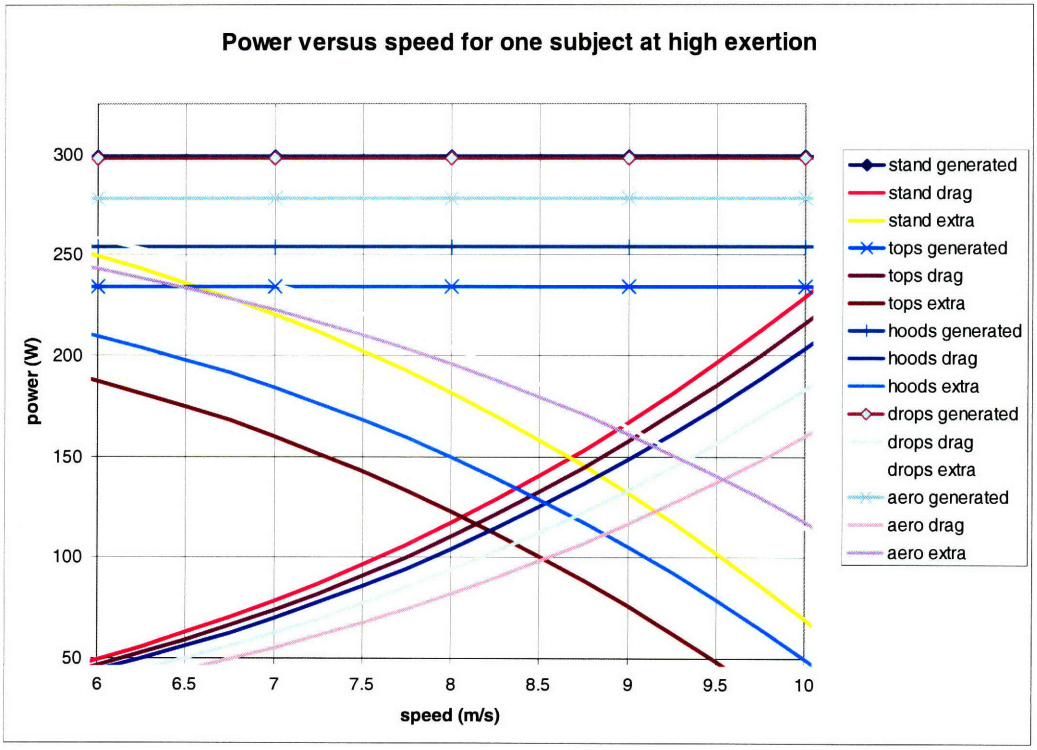

Figure 35: A closer view of Figure 12

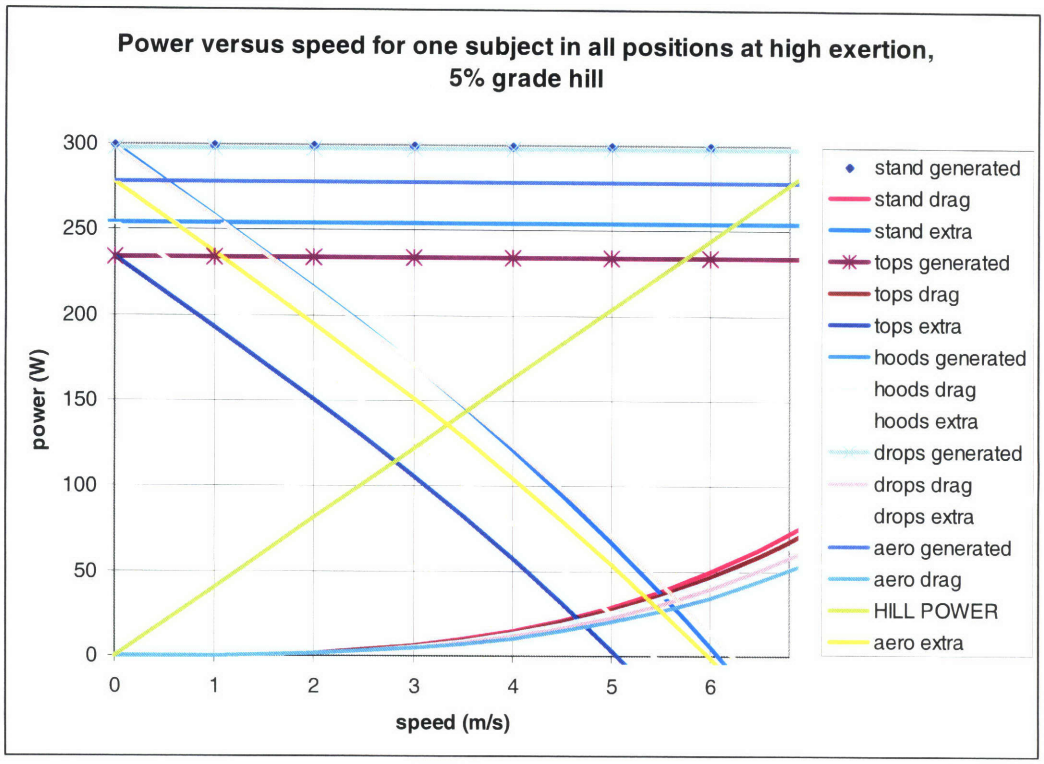

Figure 246: Predicted power vs speed curves for one subject climbing a hill at high exertion

The intersections of the excess power curves can be interpreted as position transition points. A summary of the optimal positions at each range of speeds is given in Table 3 below.

Speed range (m/s)	Hill angle (% grade)	Three optimal positions (ranked)
<6.7 (15mph)	0	1. Drops
		2. Stand
		3. Aero
6.7 (15mph)-9.5 (21.4mph)	0	1. Drops
		2. Aero
		3. Stand
>9.5 (21.4 mph)	0	1. Aero
		2. Drops
		3. Stand
<3.0 (6.75mph)	5	1. Stand
		2. Drops
		3. Aero
>3.0 (6.75 mph)	5	1. Drops
		2. Stand
		3. Aero

Table 3: Summary of position transition points for one subject pedaling at high exertion at two hill angles.

From Table 3 for a single individual, for flat ground, the most aerodynamic positions (i.e., those with lowest C_d) are more power efficient at higher speeds, as expected. At a slight incline of 5% the drops and standing positions are favored.

The power outputs averaged over everyone from Figures 30 and 31 were used to generate the power vs speed curves below. The drag coefficients in Table 2 were used to calculate the drag curves.

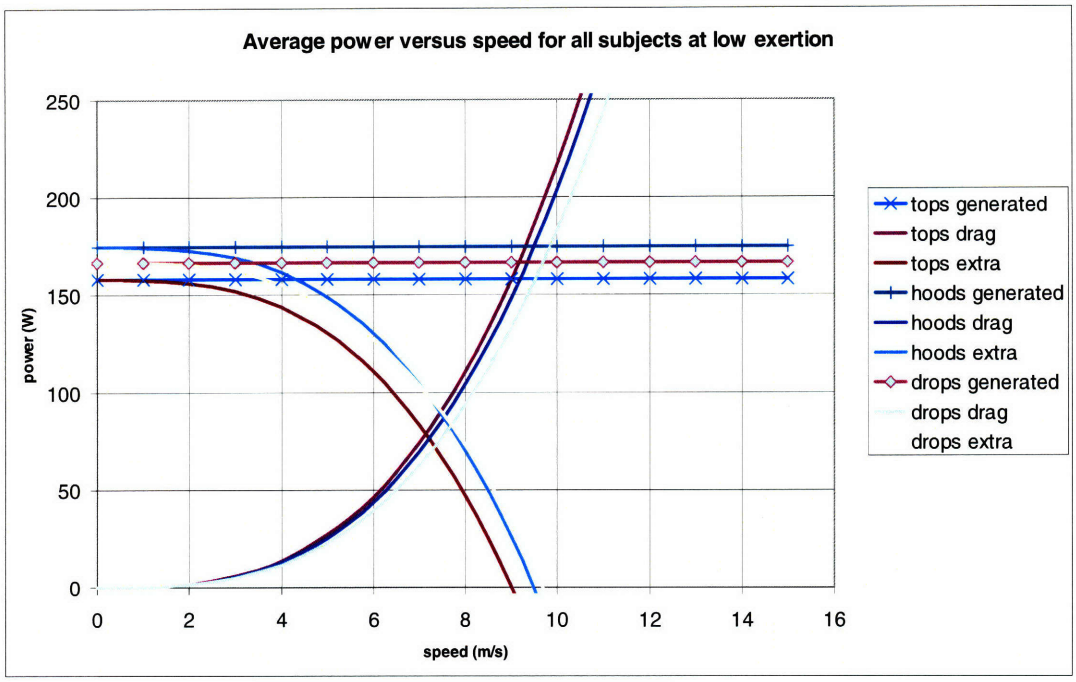

Figure 37: Predicted power averaged over all subjects versus speed, low exertion, 0% grade

Figure 38: Predicted power averaged over all subjects versus speed, high exertion, 0% grade

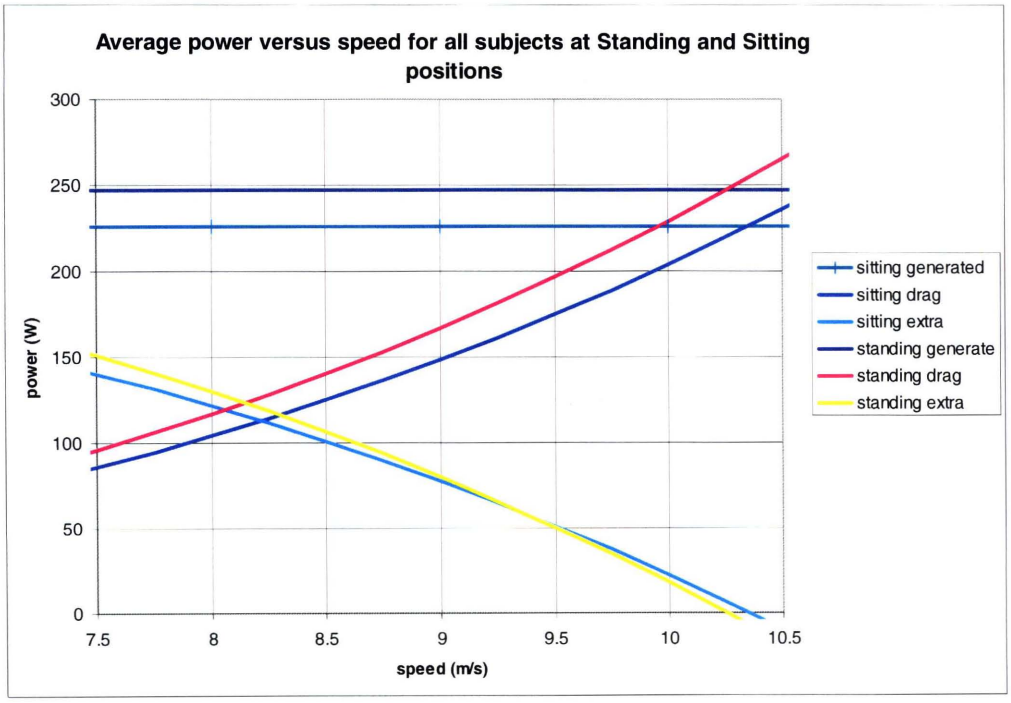

Figure 39: Predicted power averaged over all subject versus speed, standing and sitting positions, 0% grade

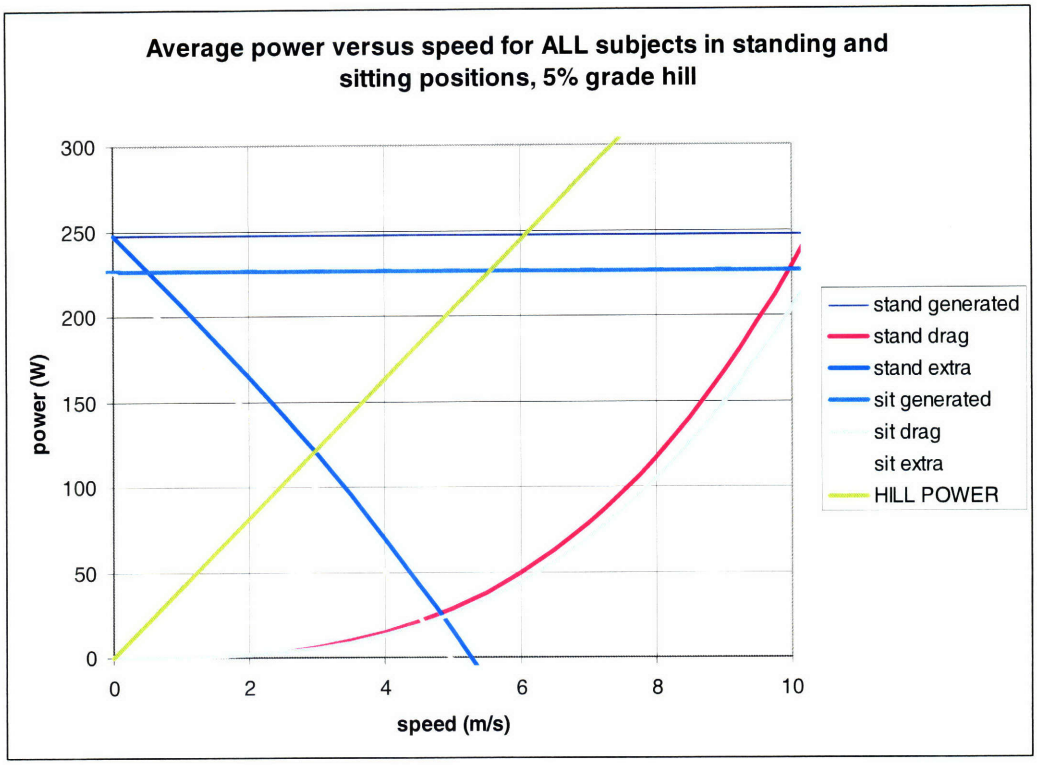

Figure 40: Predicted power averaged over all subject versus speed, standing and sitting positions, 5% grade

The predicted position transition points averaged over all subjects for a range of speeds is shown in Table 4 below.

Speed range (m/s)	Exertion level	Hill angle (% grade)	Optimal positions (ranked)
<7.0	Low	0	1. Hoods
			2. Drops
			3. Tops
>7.0	Low	0	1. Drops
			2. Hoods
			3. Tops
<6.1	High	0	1. Tops
			2. Hoods
			3. Drops
6.1-9.4	High	0	1. Drops
			2. Tops
			3. Hoods
>9.4	High	0	1. Drops
			2. Hoods
			3. Tops

<9.4	Sitting/Standing	0	1. Stand 2. Sit
>9.4	Sitting/Standing	0	1. Sit 2. Stand
All speeds	Sitting/Standing	5	1. Stand 2. Sit

Table 4: Summary of position transition points for all subjects at low and high exertion, for 0% and 5% hill grades

From Table 4, just as in Table 3 for one cyclist, the most aerodynamic position (drops) is favored at high speeds for flat ground, while standing is favored over sitting for moderately steep hills.

7.5 Cadence

The average cyclist cadence (pedal stroke frequency) was computed for three types of bikes in both the low and high exertion scenarios. The number of flashes per cycle were calculated then compared with the LED flashing frequency of 46Hz to determine pedaling frequency. The results are shown below in Table 5.

	Low Exertion		High Exertion	
Bike type	Cadence (Hz)	Standard dev	Cadence (Hz)	Standard dev
Road (7)	1.26	0.25	1.63	0.16
Triathlon (2)	1.16	0.05	1.32	0.06
Mountain (2)	1.06	0.10	1.40	0.28

Table 5: Low- and high-exertion cadences averaged over all cycling positions for three different types of bikes. The number of subjects with each type of bike is shown in parenthesis.

On average the road cyclists pedaling at high exertion had the fastest cadence: 1.63Hz ± 0.16Hz. The lowest average cadence was found to be 1.06Hz ± 0.10Hz, for mountain bikes at low exertion.

Chapter 8: Discussion

Analyzing kinematics data can offer insights into cyclist motions that are unavailable from ordinary static bicycle fits. By investigating joint angles throughout the entire pedal stroke it is possible to find angle ranges, maxima, and minima and investigate the correlation between these angles and power output. In this experiment it

was found that the wide variations in hip and ankle angle behavior between subjects have a role in determining power output. Across all subjects, knee angles were found to behave relatively similarly, suggesting that knee angles may be more finely tuned or constrained across different cyclists.

The time-varying 3D kinematics data were used to investigate out-of-plane angle motions, whose effect on power output is not yet fully understood. It was found in this study that the knee exhibits the greatest out-of-plane excursions, between 0.15" and 0.22". These data suggest that conventional bike fits that use the static position of the cyclist may need to consider kinematics analysis as well. Perhaps not just the ankle angle, but the complete muscle/bone system can benefit from this dynamic analysis.

Aerodynamic and power analyses were used in this study to investigate position transition points, that is, the speeds at which one position becomes favored over the other in terms of excess power available. It was found that at higher speeds above about 6m/s (13.4mph) the drops position became more power-efficient that the tops and hoods positions. For climbing hills of 5% grade it was found that standing was the optimal position.

These results show that valuable insights into cycling kinematics can be gained using the inexpensive LED-based motion capture system presented in this thesis.

Chapter 9: Recommendations

There are a number of improvements that could be made to this kinematics analysis system to increase its efficiency and accuracy. Attaching the LED system to the subject's leg using Velcro required about eight minutes, and could have been sped up dramatically by giving the subjects an LED-integrated spandex-type suit to place over the leg, as some subjects suggested. In addition, the efficiency of the motion capture system could be increased dramatically if both cameras were equipped with an automatic cable release to actuate the shutters. The tracking accuracy for small-displacement joints like the ankle could also be increased by securing the LEDs more firmly to the subject's body, and by increasing the flashing frequency of the LEDs to create more data points.

The custom Matlab code, while effective, was time consuming to use. In joint traces like the knee and thigh which execute an overlapping arc, it was necessary to override automatic tracking and manually click the traces. Future versions of the code with increased automation and accuracy will greatly speed up the data analysis process.

This experiment has shown the need for a more in-depth analysis of the correlation between knee and ankle angle and power output. Also of interest in future studies would be the possible negative side effects of out-of-plane knee excursions. These two variables suggest that future work on bike fits should include actual kinematics data, not just static body angles.

High-fidelity kinematics analysis should involve the use of high frame-rate digital cameras; however the current system is sufficient for low-cost initial investigations and amateur cyclists without access to advanced resources.

Chapter 10: Future Work

The kinematics analysis tools developed in this experiment can be used to analyze the motions associated with other sports. Golf swing analysis, baseball pitch analysis, and running/walking gait analysis are examples of potential analyses which can be performed without significant system modifications. Figure 41 below shows an example image taken of a golf swing using this system. The LED circuit was attached to the golfer's shoulder, hand, and along the length golf club. An automatic on-switch and off-switch could be devised to capture exactly one full golf swing, in a similar way that the switching system was used in this experiment to capture one full pedal stroke. The analysis of running and golfing data, similar to the image shown below, is a subject for future investigation.

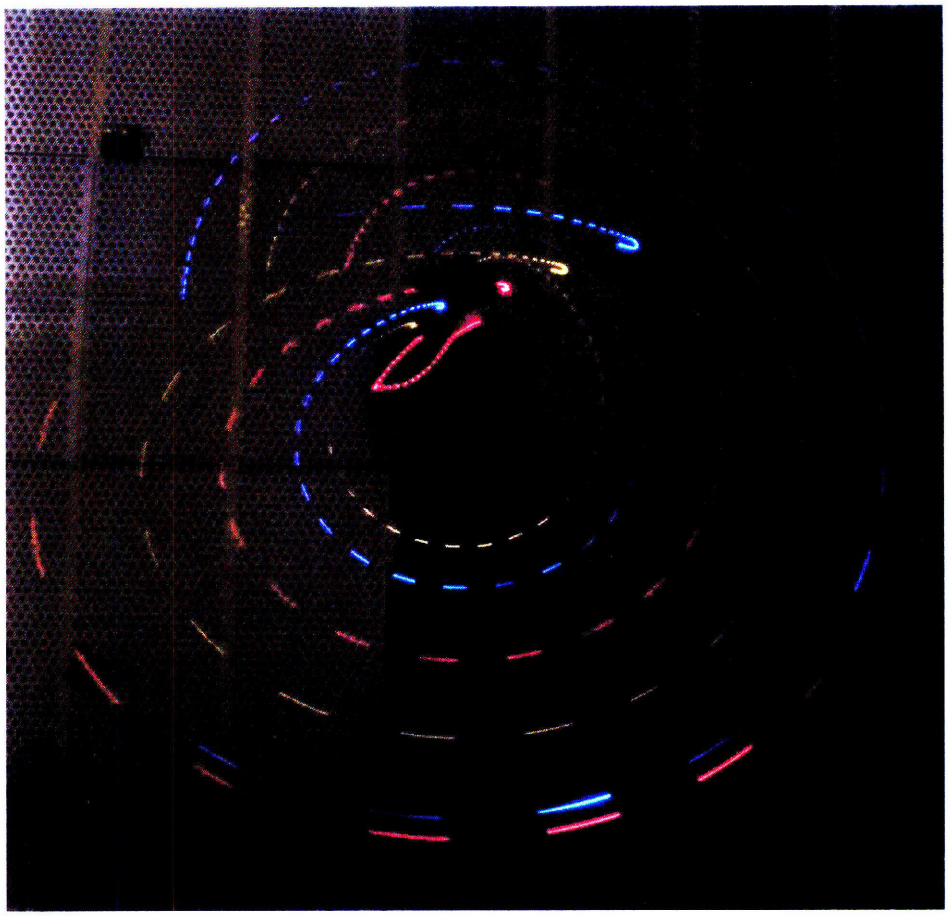

Figure 41: Using the flashing LED system, it is possible to capture the motions in other sports. In this photograph the swing of a golf club is captured in a single view. The use of multiple cameras and a higher frequency LED flashing rate would result in an accurate, low cost analysis system for golf swing analysis.

Chapter 11: References

[1] The Vicon system: http://www.vicon.com/products/performancepack.html. May 2008.

[2] J. Lee, I. Ha, Real-Time Motion Capture for a Human Body using accelerometers

[3] www.retul.com. May 2008.

[4] See, for example: Wilson, David Gordon (2004). *Bicycling Science, 3rd Ed.* MIT Press. Cambridge, MA.

[5] http://www.retul.com/the-science.asp Feb 2008.

[6] Heil, D.P.; Derrick, T.R.; Whittlesey, S. (1997). "The relationship between preferred and optimal positioning during submaximal cycle ergometry" Eur J Appl Physiol (1997) 75: 160 – 165.

[7] CycleOps Company, http://www.cycleops.com/ May 2008.

[8] http://ourworld.compuserve.com/homepages/Bill_Bowden/555.htm May 2008.

[9] Abdel-Aziz, Y.I., & Karara, H.M. (1971). Direct linear transformation from comparator coordinates into object space coordinates in close-range photogrammetry. Proceedings of the Symposium on Close-Range Photogrammetry (pp. 1-18). Falls Church, VA: American Society of Photogrammetry.

[10] Hatze, H. (1988). High-precision three-dimensional photogrammetric calibration and object space reconstruction using a modified DLT-approach. J. Biomech 21, 533-538.

Chapter 12: Appendices

12.1 Procedures

12.1.1 Wind tunnel procedure

Two cyclists were tested in MIT Wind Tunnel. A similar procedure to that outside the wind tunnel was followed while the flow was set to 30 mph and 20mph. Drag force data from the force balance were recorded every second and averaged over thirty seconds to reduce noise. A picture of the Wind Tunnel setup is shown in Figure 42.

Figure 42: Wind tunnel testing.

12.1.2 Calculation of LED flashing frequency

To determine the actual flashing rate of the LEDs, a photographic procedure was employed using both the Olympus Stylus and Olympus Camedia cameras. This procedure was performed prior to, and following the experimental data collection. First, the LEDs were activated in a dark room. One of the cameras was pointed at the LEDs and then panned slowly. As the camera panned the shutter button was pressed, and the camera continued panning until the shutter closed. As a result, photographs were generated showing the LED flashes. The number of flashes was counted and then divided by the

camera's exposure time, giving the flashing frequency. This procedure was repeated all of the cameras, and both gave a frequency of 45-46Hz.

12.1.3 Calibration Procedure

As often as possible (usually after each subject) the three dimensional calibration was performed using LEDs separated by known distances. This provided a calibration for each subject incase one of the cameras was bumped or malfunctioned midway through the experiment. To do this, the room lights were dimmed and the curtain of 1ft-spaced LEDs was suspended in a notch in the top of the calibration cube. One photograph was recorded by each camera for each position of the known LED curtain locations. The LEDs were placed in each of the six positions, all 1ft apart. A total of twelve photographs were recorded. The total time taken to record the calibration was less than five minutes.

12.2 Cost Analysis

Electronic components (LEDs, resistors, capacitors, relays, wires, breadboards, buttons, electrical tape)	$50
Velcro	$8
Trash bags	$1
PVC	$30
TOTAL COST	**$89**

Additional equipment:

Cycle trainer

Power tap wheel

Tripods

Cameras